# UNIVERSIDAD DE INVESTIGACIÓN DE TECNOLOGÍA EXPERIMENTAL YACHAY

**Escuela de Ciencias Biológicas e Ingeniería**

## TÍTULO: Enhancing Alzheimer's Diagnosis: Role of 3D Convolutional Neural Networks in MRI Analysis

Trabajo de integración curricular presentado como requisito para la obtención del título de Ingeniera Biomédica

**Autor/a:**

Pilacuan Medina Genesis Michell

**Tutor/a:**

Ph.D. Almeida Galarraga Diego Alfonso

Urcuquí, diciembre 2024

# Autoría

Yo, PILACUAN MEDINA GENESIS MICHELL, con cedula de identidad 1750690586, declaro que las ideas, juicios, valoraciones, interpretaciones, consultas bibliográficas, definiciones y conceptualizaciones expuestas en el presente trabajo; así como, los procedimientos y herramientas utilizadas en la investigación, son de absoluta responsabilidad de el/la autor/a del trabajo de integración curricular. Así mismo, me acojo a los reglamentos internos de la Universidad de Investigación de Tecnología Experimental Yachay.

Urcuquí, diciembre 2024.

_____

Genesis Michell Pilacuan Medina

CI: 1750690586

# Autorización de publicación

Yo, PILACUAN MEDINA GENESIS MICHELL, con cedula de identidad 1750690586, cedo a la Universidad de Investigación de Tecnología Experimental Yachay, los derechos de publicación de la presente obra, sin que deba haber un reconocimiento económico por este concepto. Declaro además que el texto del presente trabajo de titulación no podrá ser cedido a ninguna empresa editorial para su publicación u otros fines, sin contar previamente con la autorización escrita de la Universidad.

Asimismo, autorizo a la Universidad que realice la digitalización y publicación de este trabajo de integración curricular en el repositorio virtual, de conformidad a lo dispuesto en el Art. 144 de la Ley Orgánica de Educación.

Urcuquí, diciembre 2024.

———————————————

Genesis Michell Pilacuan Medina

CI: 1750690586

# Agradecimiento

Deseo expresar mi profundo agradecimiento a mi familia por su apoyo y comprensión incondicionales a lo largo de este proyecto. Además, extiendo mi más sincero agradecimiento a mi tutr por su invaluable orientación, paciencia y tutoría.

Génesis Michell Pilacuán Medina

# Resumen

La enfermedad de Alzheimer, un trastorno neurodegenerativo progresivo, representa un gran desafío para la salud a nivel mundial y tiene un profundo impacto en individuos, familias y sistemas de salud. Un diagnóstico temprano y preciso es esencial para un tratamiento y manejo efectivos. Este estudio se enfoca en utilizar redes neuronales convolucionales 3D para mejorar el proceso de diagnóstico del Alzheimer mediante escáneres de resonancia magnética, con el objetivo de aumentar la precisión de detección y contribuir a mejores resultados para los pacientes. Utilizando tecnologías avanzadas de imagen y redes neuronales, la investigación ofrece perspectivas prometedoras sobre métodos innovadores para detectar el Alzheimer. El rendimiento del modelo propuesto está respaldado por técnicas de preprocesamiento. El modelo alcanza una precisión de entrenamiento del 93.03%, con valores correspondientes de precisión, sensibilidad y AUC del 92.51%, 92.21% y 97.80%, respectivamente. La precisión del modelo se confirma aún más durante la validación, manteniendo una alta precisión del 88.05%, con precisión y sensibilidad ambas del 87.50%.

**Palabras Clave:** Enfermedad de Alzheimer, Redes Neuronales Convolucionales 3D, Resonancia Magnética, Neuroimagen, Segmentación de Escáneres Cerebrales, Trastornos Neurodegenerativos**.**

# Abstract

Alzheimer's Disease, a progressive neurodegenerative disorder, presents a significant challenge to global health, profoundly impacting individuals, families, and healthcare systems. Early and accurate diagnosis is essential for effective treatment and management. This study focuses on the use of 3D Convolutional Neural Networks to enhance the diagnostic process of Alzheimer's using MRI scans, aiming to improve detection accuracy and contribute to better patient outcomes. By utilizing advanced imaging and neural network technologies, the research offers promising perspective about innovative approaches for Alzheimer's detection. The performance of the proposed model is supported by thorough pre-processing and augmentation techniques. The model achieves a training accuracy of 93.03% with corresponding precision, recall, and AUC values of 92.51%, 92.21%, and 97.80%, respectively. The accuracy of the model is further confirmed during validation, maintaining high accuracy at 88.05%, with precision and recall at 87.50%.

**Keywords:** Alzheimer's Disease, 3D CNNs, MRI, Neuroimaging, Brain Scan Segmentation, Neurodegenerative Disorders.

.

# Contents

# List of Figures

# List of Tables

# Acronyms and Abbreviations

**ACh** Acetylcholine

**AD** Alzheimer's Disease

**AD8** Ascertain Dementia 8-item Informant Questionnaire

**ADNI** Alzheimer's Disease Neuroimaging Initiative

**A-IADL-Q** Amsterdam Instrumental Activities of Daily Living Questionnaire

**AIBL** Australian Imaging, Biomarkers & Lifestyle

**ALT** Alanine Transaminase

**AP** Average Precision

**ApoE** apolipoprotein E

**ASL** Arterial spin labelling

**AST** Aspartate Transaminase

**AUC** Area Under the Curve

**BET** Brain Extraction Tool

**BOLD** Blood-oxygen-level dependent

**CBIR** Content-Based Image Retrieval

**CNN** Convolutional Neural Network

**CRP** C-Reactive Protein

**CSF** Cerebrospinal Fluid

**CT** Computed Tomography

**DTI** Diffusion Tensor Imaging

**DWI** Diffusion-Weighted Imaging

**EPAD** European Prevention of Alzheimer's Dementia Consortium

**ESR** Erythrocyte Sédimentation Rate

**FAQ** Functional Activities Questionnaire

**FAST (utility)** FMRIB's Automated Segmentation Tool

**FAST (test)** Functional Analysis Screening Tool

**FDA** Food and Drug Administration

**FDG-PET** fluorodeoxyglucose-PET

**FLAIR** Fluid Attenuated Inversion Recovery

**FLIRT** FMRIB's Linear Image Registration Tool

**fMRI** Functional MRI

**FMRIB** Functional Magnetic Resonance Imaging of the Brain

**FNIRT** FMRIB's Non-Linear Image Registration Tool

**FNN** Feedforward Neural Network

**FSL** FMRIB Software Library

**FT4** Free thyroxine

**GAN** Generative Adversarial Network

**GDS** Geriatric Depression Scale

**GM** Grey Matter

**GRE** Gradient Recalled Echo

**GRU** Gated Recurrent Unit

**Hb** Hemoglobin

**HbA1c** Glycolated hemoglobin, Hemoglobin A1c

**IADL** Instrumental Activities of Daily Living

**IQCODE** Informant Questionnaire on Cognitive Decline in the Elderly

**IWG** International Working Group

**LDL** Low-density lipoprotein

**LSTM** Long Short-Term Memory Network

**MBI** Mild behavioral impairment

**MCI** Mild cognitive impairment

**Mini-Cog** Mini Cognitive Assessment Instrument

**MMSE** Mini-Mental State Examination

**MNI** Montreal Neurological Institute

**MoCA** Montreal Cognitive Assessment

**MRA** Magnetic Resonance Angiography

**MRI** Magnetic Resonance Imaging

**NIA-AA** National Institute on Aging - Alzheimer's Association

**NIfTI** Neuroimaging Informatics Technology Initiative

**NMDA** N-Methyl-D-aspartic acid

**NPI-Q** Neuropsychiatric Inventory Questionnaire

**OASIS** Open Access Series of Imaging Studies

**PET** Positron Emission Tomography

**PR** Precision-Recall

**PT** Prothrombin time

**p-tau** phosphorylated tau

**PUP** PET Unified Pipeline

**RBC** Red blood cells

**ReLU** Rectified linear unit

**RF** Random Forest

**RNN** Recurrent Neural Network

**ROC** Receiver Operating Characteristic

**SAE** Stocked Autoencoders

**SPECT** Single Photon Emission Computed Tomography

**SVM** Support Vector Machine

**SWI** Susceptibility-Weighted Imaging

**T3** Triiodothyronine

**TOF** Time of flight

**TSH** Thyroid stimulating hormone

**t-tau** total tau

**WBC** White blood cells

**WM** White Matter

# Chapter 1

# Introduction

Alzheimer's disease (AD) stands as a challenge within the realm of public health and medical research. It is a progressive and complex neurological disorder that deteriorates cognitive functions, memory, and overall mental abilities. The irreversible nature of this condition profoundly affects not only those diagnosed but also places a considerable emotional, social, and economic burden on their families and society at large [1]. As the population ages, the occurrence of this illness, typically impacting individuals in later stages of life, is increasing. Therefore, urgent advances in diagnosis and treatment are necessary.

Despite decades of research, AD continues to be a significant challenge for both clinicians and researchers. The complexity of the brain, the delayed appearance of symptoms, and the lack of precise diagnostic tests in the early stages of the disease make timely intervention and accurate diagnosis challenging [2]. Current treatments focus on alleviating symptoms and temporarily improving cognitive function, but they do not offer a cure or stop the disease's progression [2].

In recent years, efforts to better understand AD have led to advances in biomarker research, neuroimaging techniques, and a deeper comprehension of the molecular

mechanisms involved in the disease process. However, the increasing prevalence of AD far exceeds the availability and pace of treatments and research [3].

## 1.1    Problem Statement

Current diagnostic methods for Alzheimer's Disease face several challenges that slow the early and accurate identification of the condition. One significant challenge lies in the lack of methods capable of early detection, an essential factor in effectively managing the disease [2]. By the time symptoms become evident, irreversible damage to the brain may have already occurred. Additionally, the clinical presentation of Alzheimer's varies widely among individuals, making it challenging to establish a standardized set of diagnostic criteria [4], [5]. This variability leads to delayed or inaccurate diagnoses, delaying the initiation of appropriate interventions.

Imaging techniques, including Magnetic Resonance Imaging (MRI) and Positron Emission Tomography (PET) scans, are commonly used in diagnosis, but they have limitations. These techniques may lack the sensitivity to detect subtle changes in the early stages of the disease, and can sometimes produce false positives or false negatives, leading to potential misdiagnosis. Additionally, these techniques can be expensive, time-consuming, and may require specialized facilities and trained personnel, limiting their accessibility in certain regions or healthcare settings. Furthermore, some diagnostic procedures, like cerebrospinal fluid (CSF) analysis, are invasive and may not be suitable for routine screening due to their discomfort and potential risks. Moreover, CSF analysis can also be poorly available in community health facilities, further limiting its widespread utilization in diagnostic protocols [6]. Considering general medical practice and standard of care  the use of CSF or amyloid PET biomarkers have consistently led to the same conclusion: that the routine use of these biomarkers in clinical practice cannot be recommended [5].

Using Convolutional Neural Networks (CNNs) in current diagnostic methods for AD presents a promising avenue for addressing the challenges. Furthermore, 3D CNNs excel in processing three-dimensional data, providing a comprehensive analysis of structural changes in the brain [7], [8]. This capability is particularly advantageous for identifying subtle alterations in brain morphology that may occur in the various stages of Alzheimer's. Additionally, 3D CNNs can automate the analysis process, reducing the

subjectivity associated with traditional cognitive evaluations and providing a more standardized and objective approach to diagnosis [8].

Integrating 3D CNNs into diagnostic protocols can enhance Alzheimer's diagnostics by providing a tool that improves sensitivity, specificity, and objectivity in identifying the disease's manifestations. As technology continues to advance, the role of 3D CNNs in Alzheimer's diagnosis holds great promise for transforming the landscape of neurodegenerative disease detection.

## 1.2   Objectives

### 1.2.1   General Objective

Enhance detection of Alzheimer's disease by combining segmentation of brain MRI scans into three tissue types (cerebrospinal fluid, white matter, and gray matter) with the analysis capabilities of a 3D Convolutional Neural Network.

### 1.2.2   Specific Objectives

- Create a 3D Convolutional Neural Network model tailored for analyzing T1-weighted MRI scans to detect Alzheimer's Disease.
- Implement segmentation techniques during pre-processing of T1-weighted MRI scans to improve data quality and relevance for the 3D CNN model.
- Assess the model's accuracy in diagnosing Alzheimer's disease and compare its performance with traditional diagnostic methods.

# Chapter 2

# State of the Art

## 2.1   Alzheimer's Disease

Alzheimer's disease is a neurological disorder characterized by the gradual decline of cognitive function, particularly memory loss, and the inability to perform everyday activities. Named after the German psychiatrist Alois Alzheimer, who first identified the disease in 1906, Alzheimer's has become a significant global health concern with profound societal implications [9]. The global prevalence of AD is on the rise, mainly due to aging populations in many countries. According to the World Health Organization, more than 55 million people worldwide are experiencing dementia in 2023, with AD accounting for the majority [10]. Each year, nearly 10 million new cases are reported. With the aging population trend projected to continue, these numbers are anticipated to escalate, increasing the urgency for effective interventions, treatments, and preventive strategies.

Alzheimer's prevalence trends from 1990 to 2019 (Fig 2.1) depict a significant rise in the number of AD cases globally, with the prevalence in 2019 being 160.84% higher than that observed in 1990 [11].

## Alzheimer's Prevalence, 1990 to 2019
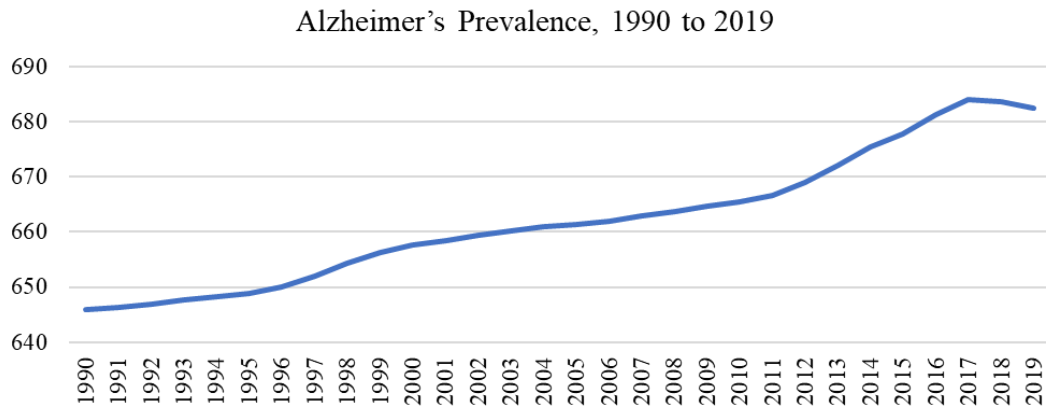


Figure 2.1 Global Prevalence of Alzheimer's Disease and Dementia (1990-2019). Number of people with Alzheimer's disease or other forms of dementia per 100,000 people aged age-standardized. Data sourced from Our World in Data [12].

In addition to the historical trend, the prevalence of Alzheimer's disease in 2019 (Fig 2.2) provides insights into the current landscape of this condition. Countries such as Turkey, Bahrain, and Kuwait reported the highest prevalence rates, while India, Nigeria, and Pakistan had comparatively lower rates [11]. Some regions, including Taiwan, China, Japan, and China, saw rapid increases in prevalence rates, showing the need for targeted interventions and resource allocation in these areas [11]. On the other hand, countries like Luxembourg, Nigeria, and Spain experienced notable decreases in prevalence rates, indicating potential success in combating the prevalence of AD [11]. Understanding these patterns is key to developing effective healthcare interventions and strategies aimed at addressing the current impact of Alzheimer's disease worldwide.

## Alzheimer's Prevalence
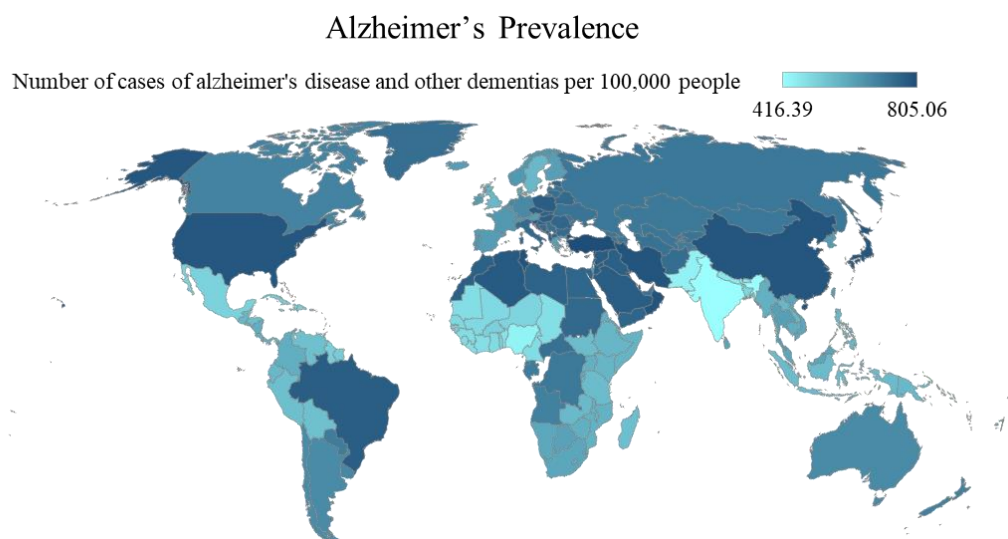


Figure 2.2 Global Prevalence of Alzheimer's Disease and Dementia (2019): Age-Standardized Cases per 100,000 People - Data sourced from Our World in Data [12].

The impact of Alzheimer's extends beyond individuals to their families, caregivers, and society at large. It is not merely a disease of memory; it affects a person's ability to reason, communicate, and carry out daily tasks. Families often bear a substantial emotional and financial burden, as the disease needs long-term care, leading to increased healthcare costs and stress on caregivers.

Moreover, the escalating prevalence of AD globally presents an immense challenge for healthcare systems [13]. The intricate nature of the disease requires a detailed approach including medical and social care. From initial diagnosis through to long-term support, healthcare providers struggle with the many demands of Alzheimer's, requiring innovative solutions and an evolution in care delivery models. This strain on healthcare infrastructure is particularly pronounced, especially with more elderly people needing care [13]. This emphasizes the need for careful planning and distributing resources to handle the increasing demand for Alzheimer's care.

Beyond the healthcare sector, the economic reverberations of Alzheimer's are profound. The financial burden extends beyond direct healthcare costs, encompassing lost productivity and wages as individuals exit the workforce or reduce work hours to care for affected family members [14]. The World Health Organization indicates that in 2019, dementia posed a global economic burden of 1.3 trillion dollars, and approximately half of these costs were associated with informal care [10]. However, when considering vascular dementia alongside Alzheimer's, the total rises to $2.8 trillion, calculated in 2020 US$ [15]. Projections (Fig. 2.3) suggest a pronounced increase, with the global economic burden forecasted to reach $4.7 trillion by 2030, $8.5 trillion by 2040, and $16.9 trillion by 2050. The largest proportional increases are expected in low-, lower-middle-, and upper-middle-income countries, while high-income countries are less affected. These projections augment the urgent need for effective interventions and policies to address the escalating economic burden of AD and related dementias globally.

Estimated economic burden of Alzheimer's disease and related dementias, 2019-2050
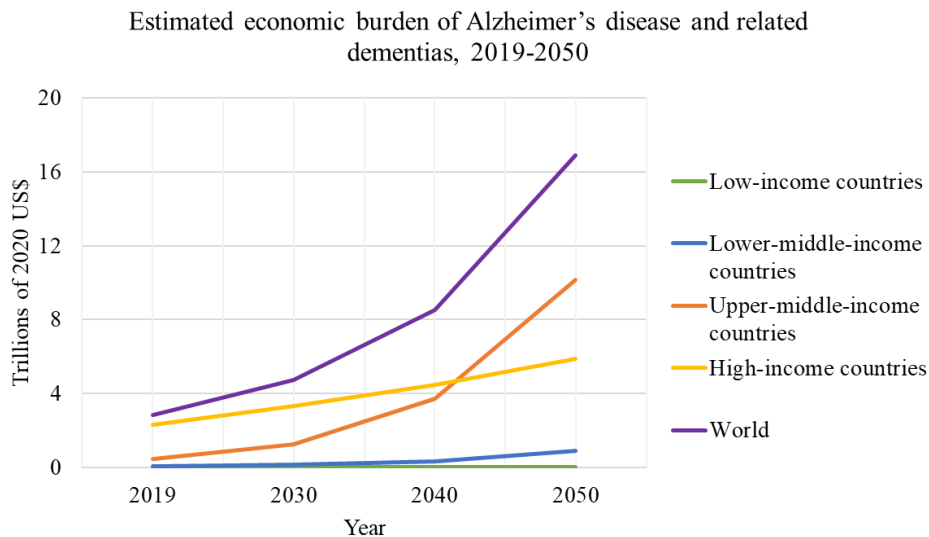


Figure 2.3 Estimated economic burden of Alzheimer's Disease and related dementias by country groups (2019-2050), trillions of 2020 constant US$ [15].

Concurrently, research and development efforts are intensifying as the race to understand the complexities of Alzheimer's becomes a focal point in medical research [13]. In addition to these efforts, It is increasingly important to make more people aware and break down the negative views linked to Alzheimer's [13]. Reducing the societal taboo surrounding the disease can not only encourage early diagnosis but also create a more compassionate environment, enhancing support for those affected and their families.

Alzheimer's is a progressive disease, intensifying over time, with pace and declining abilities varying among individuals. As the disease advances, more neurons succumb to damage, impacting broader areas of the brain [3]. Consequently, heightened assistance from family, friends, and professional caregivers becomes imperative for individuals to carry out daily activities to ensure their safety. The trajectory of Alzheimer's may also include changes in mood, personality, and behavior [14]. As the disease relentlessly progresses, the neuronal damage extends to vital brain regions governing essential bodily functions like walking and swallowing. Individuals eventually become bed-bound, necessitating round-the-clock care [14]. The changes in the brain linked to Alzheimer's disease are the primary factors leading to dementia. These changes have widespread effects on memory, cognition, sensory perception, emotions, motor skills, and abilities.

The cellular basis of the brain changes associated with AD has been extensively studied. It involves the accumulation of beta-amyloid fragments into clumps outside neurons (beta-amyloid plaques) and the abnormal hyperphosphorylation of the tau protein, which leads to the formation of tangles inside neurons (tau tangles) (Fig. 2.4) [16]. These alterations precede the damage and the destruction of neurons, known as neurodegeneration, a crucial element in Alzheimer's pathology [3]. The roles of beta-amyloid and tau in Alzheimer's are distinctive. Beta-amyloid plaques and accumulations may hinder neuron-to-neuron communication, impacting synapses [16]. Tau tangles inside neurons obstruct nutrient transportation, which is vital for neuron function and survival [3]. The complete understanding of the sequence of events or exact mechanisms is still unclear [16].
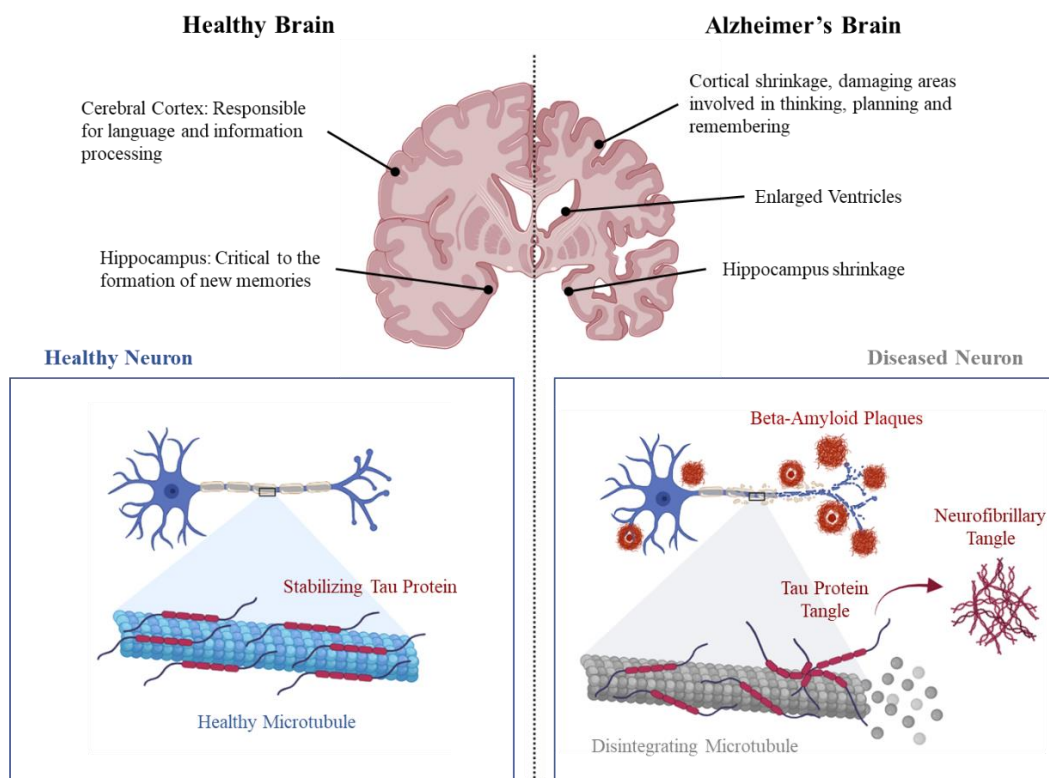


Figure 2.4 Comparative Illustration of Healthy vs. Diseased Brain in Alzheimer's Disease.

Other Alzheimer 's-associated brain changes involve inflammation and decreased brain volume (atrophy). The presence of toxic beta-amyloid and tau proteins activates immune system cells called microglia, attempting to clear these proteins and cellular debris [17]. Chronic inflammation may ensue when microglia struggle to keep pace, contributing to atrophy caused by cell loss [17]. Compounded by diminished glucose metabolism, normal brain function is further compromised [14].

Advancements in research have enable the measurement of these brain changes, incrementing the understanding of the disease's pathology. Identifying abnormal beta-amyloid and tau levels in CSF and utilizing PET for imaging has become instrumental in diagnosing and understanding Alzheimer's [18]. These accumulations serve as biomarkers, measurable biological changes indicating the presence or risk of AD. Such advancements not only enhance our understanding of Alzheimer's but also offer potential avenues for early detection and intervention, essential elements in efforts to combat this neurodegenerative disorder.

### 2.1.1   Importance of Early Diagnosis

The significance of early and accurate diagnosis in Alzheimer's disease goes beyond clinical identification, serving as a starting point for effective intervention and management strategies. The timely recognition of Alzheimer's not only provides knowledge about the condition and the patient but also gives avenues for targeted interventions capable of mitigating the progression of the disease.

Early diagnosis facilitates the initiation of treatments, enabling healthcare providers to introduce therapeutic strategies that include medications, cognitive rehabilitation, and lifestyle modifications [4]. This approach, made for the individual's evolving needs, aims not just to treat symptoms but to create a comprehensive care plan that fits the individual's situation. Importantly, this encompasses not only the medical dimension but also the psychosocial and emotional aspects, acknowledging the profound impact Alzheimer's has on both individuals and their families.

Beyond just direct medical treatment, an early diagnosis is the foundation for care planning [19]. It gives families a head start to plan and handle Alzheimer's challenges, from legal and financial considerations to long-term care preferences [20]. This planning, based on early diagnostic, gives power to individuals and their families to make informed decisions. Moreover, it also opens doors to education and support services for caregivers, which can significantly ease the burden and stress associated with caregiving, enhancing the overall quality of life for individuals with Alzheimer's and their support systems [20].

Participation in clinical trials and research studies represents another facet of the early diagnosis paradigm [21]. Individuals identified early with AD can contribute to the advancement of scientific understanding while gaining access to experimental treatments and therapies that may hold promise for altering the course of the disease. This dual role as contributors to medical knowledge and beneficiaries of new interventions shows the big potential of early diagnosis.

Beyond the clinical and research realms, early diagnosis serves as a shield against potentially reversible causes of cognitive decline [22]. By identifying factors such as medication side effects, depression, or vitamin deficiencies, healthcare professionals can offer interventions to address these specific issues, offering an individualized approach to care.

### 2.1.2   Diagnosis Approaches

Diagnosing AD involves various approaches to identify its progression and stages. One way to understand this is by recognizing the continuum of the disease, which spans from an asymptomatic phase with biomarker evidence of AD (preclinical AD) through mild cognitive impairment (MCI) and mild behavioral impairment (MBI) to the eventual development of AD dementia [4]. Various staging systems, with differing definitions for each stage, have been established to categorize AD across its progression (Fig. 2.5).
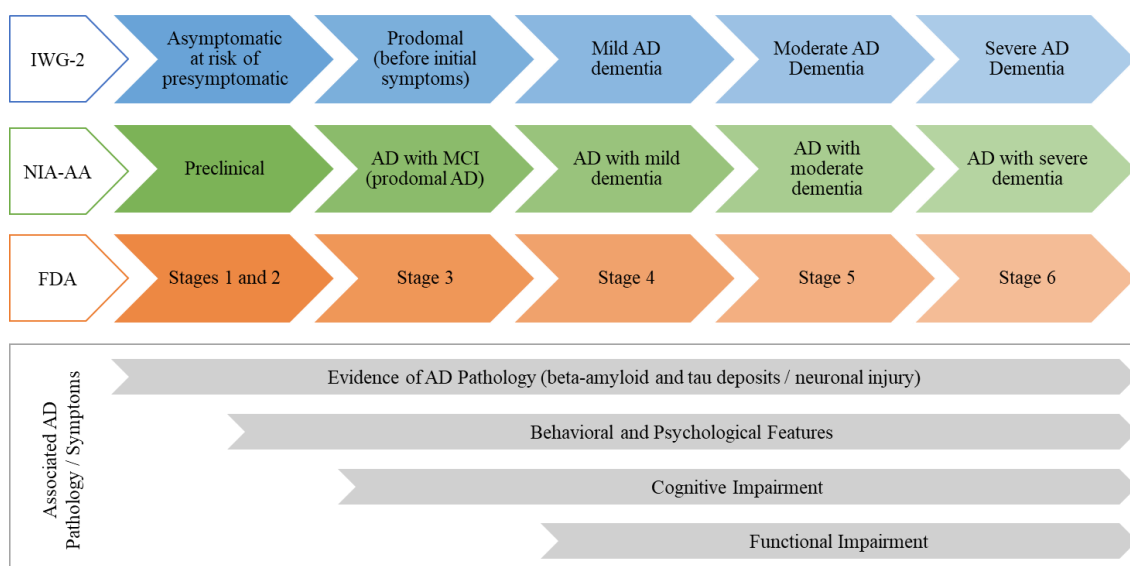


Figure 2.5 Stages of Alzheimer's Disease Progression according to Different Classifications. Adapted from Porsteinsson A.P. et al. [4].

Traditional diagnostic methods for Alzheimer's disease involve a comprehensive and multifaceted approach, including clinical assessments, cognitive tests, and neuroimaging. These methods are necessary for detecting and confirming the presence of Alzheimer's, especially in the early stages when interventions may be more effective. Table 2.1 summarizes the recommended steps to support each stage of the diagnosis process.

| | |
|---|---|
| Step 1: Detection | • Gather comprehensive patient and family history<br>• Incorporate caregiver insights<br>• Review medical and disease history<br>• Document medication regimen<br>• Assess lifestyle factors |
| Step 2: Evaluation and Differentiation | • Conduct blood tests for comprehensive analysis<br>• Consider genotyping for genetic predispositions<br>• Perform neurological and physical examinations<br>• Administer cognitive assessments<br>• Evaluate functional abilities<br>• Assess behavioral symptoms<br>• Utilize imaging techniques |
| Step 3: Diagnosis | • Employ advanced diagnostic tools:<br>  - Amyloid PET imaging<br>  - Analysis of CSF markers: $A\beta42$, p-tau, and t-tau levels<br>  - Calculate CSF $A\beta42/A\beta40$ ratio |
| Step 4: Treatment and Management | • Implement symptomatic treatments such as Ach inhibitors and NMDA receptor antagonists<br>• Recommend lifestyle modifications to support cognitive health<br>• Provide social work support and resources for caregivers<br>• Encourage participation in clinical trial registries for potential therapeutic advancements |

Table 2.1 Phases in the AD Diagnostic Process, accompanied by the Recommended Steps. Adapted from Porsteinsson A.P. et al. [4].

**2.1.2.1  Physical Examination and Blood Analyses**

A thorough physical examination and blood analyses play important roles in the diagnostic process for AD by identifying potential underlying medical conditions and reversible causes of cognitive impairment. During the physical examination, which includes mental status and neurological assessments, clinicians can detect conditions like depression and search for signs indicative of stroke or other neurological disorders [23]. Additionally, checking diet, medication history, blood pressure, temperature, pulse, and cardiovascular health can provide helpful information into a patient's overall health and potential contributors to cognitive decline. Blood tests are essential for ruling out treatable conditions that may mimic Alzheimer's or dementia symptoms, such as vitamin B12 deficiency or thyroid disease [24]. Recommended blood analyses are summarized in Table 2.2. Furthermore, genetic testing may be considered in individuals with a family history of early-onset Alzheimer's or dementia, with some clinics offering ApoE genotyping services and consumer tests becoming increasingly accessible for those interested in assessing their genetic risk for Alzheimer's disease [4].

| Test | Measurements | Abnormal results | Dementia/AD relation |
|------|--------------|------------------|----------------------|
| Complete Blood Count with Platelet Count | - RBC<br>- WBC<br>- Platelets<br>- Hb | - Anemia (low RBC or Hb)<br>- Infection (elevated WBC)<br>- Thrombocytopenia (low platelets) | Anemia may contribute to cognitive decline; infections may indicate underlying inflammation or infection-related cognitive impairment. |
| Serum Creatinine and Urea Concentration | - Creatinine<br>- Urea | - Acute or chronic kidney disease (elevated creatinine and urea) | Kidney dysfunction may lead to metabolic disturbances affecting cognition. |
| Glucose and Glycated Hemoglobin | - Blood sugar levels<br>- HbA1c | - Diabetes mellitus (elevated fasting glucose or HbA1c) | Diabetes and dysglycemia are associated with cognitive impairment and increased risk of AD. |
| Lipid Profile | - Cholesterol<br>- Triglyceride | - Dyslipidemia (elevated total cholesterol, LDL, or triglycerides) | Dyslipidemia is associated with increased risk of vascular cognitive impairment and AD. |
| Albumin | Albumin | - Liver disease (low albumin) | Liver dysfunction may impact cognitive |

| | | | function through metabolic disturbances and inflammation. |
|---|---|---|---|
| Liver Assessment with Transaminases and Prothrombin Time | - AST<br>- ALT<br>- PT | - Liver disease (elevated ALT or AST)<br>- Coagulopathy (prolonged PT) | Liver dysfunction may affect cognitive function through metabolic disturbances and inflammation. |
| Electrolyte Measurement | - Sodium<br>- Potassium<br>- Calcium | - Electrolyte imbalances (hyponatremia, hyperkalemia, hypocalcemia) | Electrolyte imbalances can lead to cognitive impairment and confusion. |
| Thyroid Hormones | - TSH<br>- FT4<br>- T3 | - Hypothyroidism (elevated TSH, low FT4)<br>- Hyperthyroidism (low TSH, elevated FT4) | Thyroid disorders can affect cognition and mimic symptoms of dementia. |
| Vitamin B12 and Folic Acid Measurement | - Vitamin B12<br>- Folate | - Vitamin B12 deficiency (low B12)<br>- Folic acid deficiency (low folic acid) | Deficiencies in vitamin B12 and folic acid can cause cognitive impairment and dementia-like symptoms. |
| Erythrocyte Sedimentation Rate and C-Reactive Protein | - ESR<br>- CRP | - Inflammatory conditions (elevated ESR or CRP) | Chronic inflammation is associated with increased risk of cognitive decline and AD. |
| Screening Tests for Main Infections | - Syphilis<br>- HIV<br>- Hepatitis B<br>- Hepatitis C. | - Positive test results indicate active infection, which may require further evaluation and treatment | Certain infections, such as HIV and syphilis, can directly affect the brain and cognitive function, leading to dementia-like symptoms. |

Table 2.2 Suggested routine laboratory tests in the diagnosis of dementia [25], [26].

### 2.1.2.2 Cognitive Testing

Cognitive testing is an important component of Alzheimer's diagnosis, aiming to determine various aspects of cognitive function. These tests measure memory, attention, language skills, and executive function. Well-established tests, such as the Mini-Mental State Examination (MMSE) and the Montreal Cognitive Assessment (MoCA), are commonly employed [27]. These assessments provide quantifiable data and help evaluate the severity of cognitive impairment. Discrepancies between an individual's current cognitive performance and their baseline or expected abilities contribute to the

diagnostic criteria for AD. Table 2.3 summarizes and compares commonly used cognitive tests.

| Test | Score | Questions or Items | Time (min) | Characteristics |
|------|-------|--------------------|------------|-----------------|
| MMSE | Lower scores indicate greater cognitive impairment. | 30 | 5-10 | - May have limitations in identifying impairments in executive functioning.<br>- Minimal training requirements.<br>- Paid test |
| MoCA | Lower scores indicate greater cognitive impairment. | 30 | 10 | - More sensitive than MMSE, particularly in detecting MCI.<br>- Minimal training requirements.<br>- Paid test |
| Mini-Cog | Scored out of 5, with 3 points for recall and 2 points for the clock-drawing task. Lower scores suggest cognitive impairment. | 3 recall items, plus clock-drawing task | 2-3 | - Involves recalling three items from a list and drawing a clock<br>- Brief assessment<br>- Easy to interpret<br>- No training requirements. |
| AD8 | Higher scores indicate more cognitive impairment. | 8 | 2-3 | - Informant questionnaire<br>- Brief assessment for cognitive impairment |
| IQCODE | Scored on a Likert scale, with higher scores indicating greater cognitive decline. | Varies (26-30) | 10 | - Measures decline from premorbid level<br>- Informant questionnaire |

Table 2.3 Comparison of Cognitive Screening Tests [4], [23], [27], [28].

### 2.1.2.3  Functional Testing

Functional testing assesses a patient's daily activities by evaluating their instrumental activities of daily living (IADL), which encompass essential tasks for independent living such as cooking, shopping, and managing finances. These activities may become impaired during the early stages of cognitive decline, particularly in neurodegenerative diseases. While some decline in instrumental activities of daily living performance is expected with normal aging, significant impairments are strongly associated with AD. Commonly used functional assessments are summarized in Table 2.4.

| Test | Score | Questions or Items | Time (min) | Characteristics |
|------|-------|--------------------|-----------|-----------------|
| FAQ | Ranges from 0 (independent) to 30 (dependent) | 10 | 5-10 | Highly reliable assessment for evaluating functional ability, focusing on a range of daily living activities. |
| A-IADL-Q | 5-point Likert scale (individual items) | 47-70 | Depends on the version of the test. | Less influenced by demographic factors. Can be sensitive to early stages of the disease. |
| FAST | Yes/No for presence of behavioral concerns | 28 | 10-15 | Identifies functional and behavioral problems through multiple informant reports. |

Table 2.4 Comparison of Functional Screening Tests [4], [23], [29].

## 2.1.2.4 Behavioral Testing

Patients suspected of having Alzheimer's disease often exhibit various behavioral symptoms, including as anxiety, depression, apathy, psychosis, and agitation [30]. These symptoms, especially prevalent in the early stages of the disease, not only contribute to poor long-term outcomes but also impose significant burden on caregivers and distress patients and their families. Clinicians are necessary for the task of distinguishing behavioral and psychiatric symptoms caused by neurodegenerative diseases like AD from those deriving from alternative causes, such as mood disorders [23]. To assess neuropsychiatric symptoms in patients with suspected early-stage AD, clinicians commonly employ the tests summarized in Table 2.5.

| Test | Score | Question or Items | Time (min) | Characteristics |
|------|-------|-------------------|-----------|-----------------|
| GDS | 0 to 3 scale. Higher scores represent the presence of more depressive symptoms | 15 or 30 | 5-10 | Self-reported questionnaire used to assess depression specifically in older adults. Questions target the individual's recent mood, with a specific emphasis on the past week. |
| NPI-Q | 1 to 3 scale. Higher scores indicate higher degree of behavioral disturbance | 12 | 5 | It is a structured interview conducted with an informant to assess the presence and severity of symptoms across 12 behavioral domains. |

Table 2.5 Comparison of Functional Screening Tests [4], [31].

### 2.1.2.5  Neuroimaging

Advancements in neuroimaging technologies have significantly enhanced the diagnostic capabilities for AD. Table 2.6 shows a summary of neuroimaging tests frequently used in AD.

| Neuroimaging Test | Brain Areas | Characteristics | Modality |
|---|---|---|---|
| MRI | Whole brain | High-resolution images of brain structure can detect brain atrophy, especially in the hippocampus. | Structural |
| fMRI | Brain Activity Regions | Measures brain activity by detecting changes in blood flow. | Functional |
| CT | Whole brain | Quick imaging can show gross structural abnormalities. | Structural |
| PET | Hippocampus, Amyloid Plaques | Can detect beta-amyloid plaques and tau tangles, which are hallmarks of Alzheimer's disease. | Molecular |
| SPECT | Cerebral Blood Flow | Shows blood flow to tissues and organs. | Functional |
| DTI | White matter tracts | Maps white matter tracts and can show connectivity loss in the brain. | Structural/ Functional |

Table 2.6 Common Neuroimaging Tests used for Alzheimer's Disease, brain areas they focus on, characteristics, and imaging modalities [24].

MRI and Computed Tomography (CT) scans provide detailed images of the brain's structure, aiding in the identification of atrophy and other abnormalities [32]. These imaging techniques assist in ruling out other potential causes of cognitive decline, such as tumors or vascular issues.

PET scans utilizing specific tracers can highlight areas of the brain with abnormal beta-amyloid deposits, one of the hallmark features of Alzheimer's [33]. Additionally, fluorodeoxyglucose (FDG)-PET scans measure glucose metabolism in the brain, helping identify regions with decreased activity, which is indicative of neuronal dysfunction [34]. These neuroimaging methods give important details about the structural and functional changes associated with Alzheimer's, supporting a more accurate diagnosis.

2.1.2.5.1    Magnetic Resonance Imaging

MRI operates on the principles of nuclear magnetic resonance, utilizing the behavior of atomic nuclei within a magnetic field. In the context of Alzheimer's disease, MRI provides very detailed information about the structural changes occurring in the brain, showing clear signs of shrinking, abnormal protein buildup, and other aspects of the disease.

The MRI process involves exposing the body, in this case, the brain, to a strong magnetic field and radiofrequency pulses. The interaction of these components with hydrogen atoms, abundant in the human body due to the prevalence of water, results in the emission of signals [35]. The detection and interpretation of these signals form the basis of MRI images. Notably, the contrast between different types of tissues within the brain enables the visualization of anatomical structures with remarkable detail. Figure 2.6 shows the different planes of the brain on a T1-weighted MRI, and the Figure 2.7 shows the slices of a brain in the axial plane.
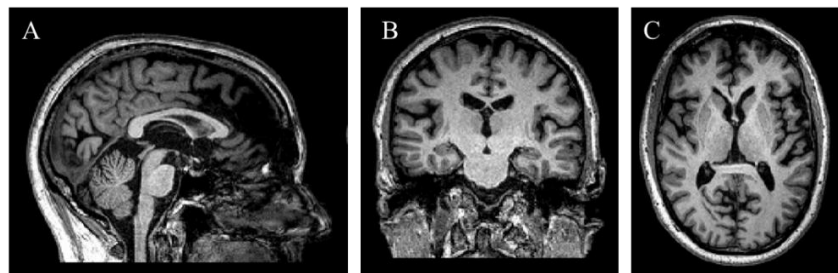


Figure 2.6 Different planes from OASIS 3 displayed in FSLeyes. A) Sagittal Plane. B) Coronal Plane. C) Axial Plane.
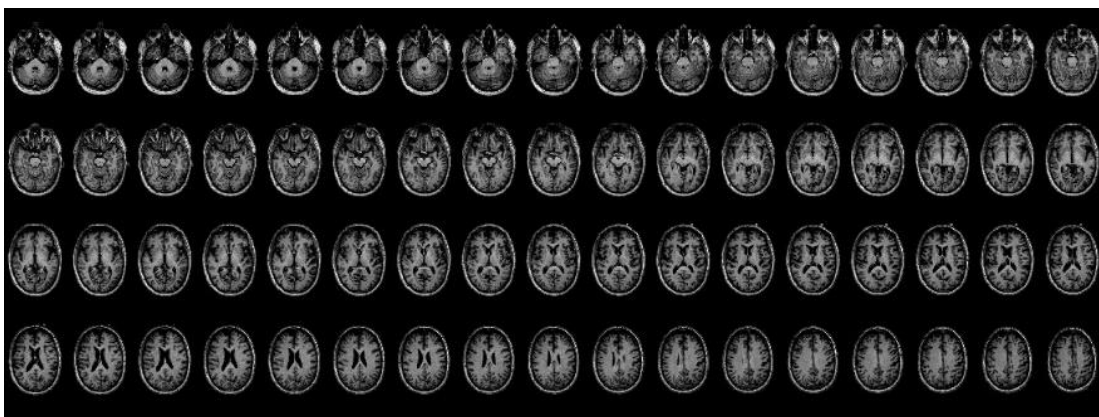


Figure 2.7 Axial View of Sequential MRI Brain Scan Slices from OASIS 3 - Lightbox Display in FSLeyes.

In the context of Alzheimer's, various MRI sequences are employed to distinguish different aspects of the disease's structural alterations. Table 2.7 summarizes the MRI sequences commonly used on the brain.

| MRI Sequence | Imaging Characteristics | Application |
|---|---|---|
| T1-Weighted (Fig. 2.8A) | - High spatial resolution<br>- Anatomical detail<br>- CSF appears dark<br>- White matter appears light | - Anatomical studies<br>- Assessment of brain atrophy<br>- Lesion detection |
| T2-Weighted (Fig. 2.8B) | - High contrast for fluid<br>- CSF appears bright<br>- White matter appears dark | - Detection of edema and inflammation<br>- Evaluation of white matter lesions<br>- Identification of acute stroke |
| T2*-Weighted (Fig. 2.8C) | - Sensitive to magnetic susceptibility<br>- Hemorrhages and calcifications appear dark<br>- Can show iron deposits and microbleeds | - Detection of blood degradation products<br>- Imaging of iron deposition in neurodegenerative diseases<br>- Evaluation of small vascular lesions |
| FLAIR (Fig. 2.8F) | - Suppresses fluid signal<br>- CSF appears dark<br>- Lesions near CSF spaces are highlighted | - Multiple sclerosis plaque detection<br>- Identification of subtle brain lesions<br>- Chronic stroke assessment |
| DWI (Fig. 2.8E) | - Sensitive to the diffusion of water molecules<br>- Acute stroke lesions appear bright | - Early stroke detection<br>- Differentiation between cytotoxic and vasogenic edema |
| GRE | - Susceptibility to magnetic field inhomogeneities<br>- Blood products and calcifications appear dark | - Detection of hemorrhage<br>- Identification of vascular abnormalities<br>- Iron deposition studies |
| SWI (Fig. 2.8D) | - Enhanced sensitivity to blood products and iron<br>- Venous structures and iron appear dark | - Detection of micro hemorrhages<br>- Venous angiography<br>- Traumatic brain injury assessment |
| MRA | - Visualization of blood flow without contrast agents<br>- Blood vessels appear bright | - Non-invasive vascular system evaluation<br>- Aneurysm and vascular malformation detection |
| fMRI | - Detects changes in blood oxygenation<br>- Highlights areas of brain activity | - Brain function mapping<br>- Pre-surgical planning<br>- Research into brain disorders |

Table 2.7 Summary of MRI Brain Sequences: Imaging Characteristics and Clinical Applications [27].
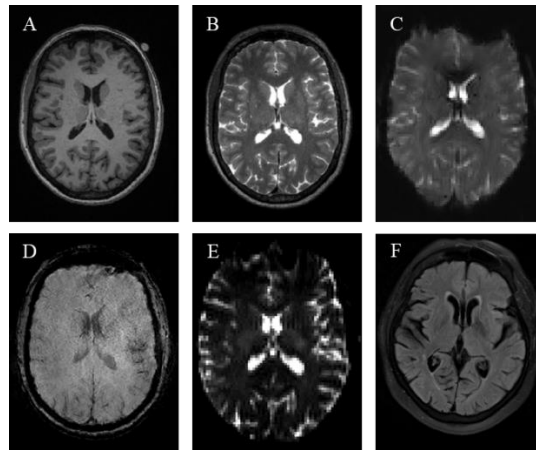
Figure 2.8 Comparison of Axial Plane MRI Sequences in Brain Imaging Displayed in FSLeyes: A) T1-Weighted, B) T2-Weighted, C) T2*-Weighted, D) SWI, E) DWI, F) FLAIR.

In essence, the nature of Alzheimer's pathology needs a specific approach, and MRI, with its diverse sequences, emerges as a versatile tool. By combining anatomical and functional information, different MRI sequences contribute to a comprehensive understanding of Alzheimer's, aiding in early diagnosis, disease monitoring, and the creation of targeted interventions. As technological advancements continue, MRI continues to be a vital tool in discovering and understanding the structural changes in the brain caused by AD, offering hope for improved diagnostics and more effective therapeutic strategies.

## 2.2    Overview of Neural Networks

### 2.2.1    Introduction

Neural networks, popular in artificial intelligence and machine learning, are designed to emulate the information processing capabilities witnessed in the human brain. These networks, inspired by their biological counterparts, are comprised of interconnected nodes, or artificial neurons, arranged into layers [36]. Much like biological neurons, these artificial counterparts receive input signals, process them through weighted connections, and produce an output signal, enabling the network to learn and make predictions.

The neural network's architecture involves distinct layers, beginning with the input layer, where external data or features are presented [36]. Hidden layers, nestled between the input and output layers, perform the bulk of the information processing, similar to the complex neural circuits in the human brain. The output layer then generates the final

result, which could be a classification, prediction, or any other desired outcome. This layered organization mirrors the hierarchical structure of the human brain and facilitates the network's capacity to capture intricate patterns within data.

The learning process in neural networks revolves around adjusting weights and biases [37]. Weights, analogous to synaptic strengths in biological systems, determine the influence of one node on another. During training, these weights are modified to optimize the network's performance, reflecting a form of artificial synaptic plasticity [38]. Biases, additional parameters within nodes, introduce flexibility, allowing the network to adapt and learn representations from the data.

Activation functions introduce non-linearity into the network. This non-linearity is essential for modeling complex relationships within data, similar to the activation of biological neurons [39]. Sigmoid, hyperbolic tangent, and rectified linear unit (ReLU) are common activation functions that determine whether a node should activate based on the weighted sum of inputs and biases.

Essentially, neural networks combine computational power with biological inspiration. They consist of interconnected nodes organized into layers, each emulating the functionality of biological neurons. The weighted connections and activation functions allow these artificial systems to learn and adapt, mirroring the plasticity observed in biological synapses. As artificial neural networks continue to evolve, inspired by the intricate workings of the human brain, they give new possibilities in the realm of artificial intelligence, propelling advancements and innovations across diverse domains.

### 2.2.2   Mechanism of Neural Networks

The forward propagation process in neural networks is the mechanism by which input data is processed layer by layer, culminating in the generation of an output [40]. This sequential flow of information through the network shows how neural networks predict or classify data accurately. This forward propagation process lays the groundwork for predictions; however, it is the backpropagation algorithm that refines the network's predictive capabilities through iterative learning. Backpropagation is a fundamental mechanism that adjusts weights and biases to minimize the discrepancy between the network's predictions and the actual output during the training phase [40].

After the forward propagation process generates predictions, the computed output is compared to the true target values. The resulting error, often quantified using a loss or cost function, serves as a measure of the disparity between the predicted and actual outcomes [41]. Backpropagation operates by propagating this error backward through the network, layer by layer, adjusting the weights and biases to reduce prediction errors systematically.

The essence of backpropagation lies in the chain rule of calculus, which enables the computation of gradients for each weight and bias with respect to the overall error [38]. Gradients represent the rate of change of the error concerning the corresponding weight or bias. The weights and biases are then adjusted in the opposite direction of these gradients, nudging the network parameters to minimize the error [38], [41].

Mathematically, the weight update can be expressed as a learning rate multiplied by the gradient of the error with respect to the weight [42]. The learning rate controls the step size of these updates, preventing the algorithm from overshooting the optimal parameter values. This iterative process continues over multiple epochs, refining the network's parameters to converge toward a state where the error is minimized.

Notably, activation functions introduce non-linearity into the network during the forward propagation process. These functions determine whether a neuron should activate based on the weighted sum of inputs and biases [39]. This non-linearity is crucial for tasks involving non-linear patterns, allowing the network to learn and represent intricate features and correlations in the input data.

The neural network learns from the training data by adjusting weights and biases during backpropagation while considering the non-linear activation functions and improving its generalization ability [41]. The adaptability of this learning process, combined with the non-linear activation functions, enables neural networks to capture complex patterns, making them versatile tools across various artificial intelligence applications. The teamwork of forward propagation, backpropagation, and activation functions highlights the network's ability to autonomously adapt and optimize its predictive capabilities over successive training iterations.

### 2.2.3    Types of Neural Networks

### 2.2.3.1    Perceptron

The perceptron is a basic type of neural network used for classifying data into two parts [43]. It works by multiplying input signals with weights, summing them up, and then passing this sum through a function that decides the output. If the sum is above a certain threshold, the perceptron activates an output; otherwise, it does not. Perceptrons are mainly used in simple tasks like image recognition [44], [45], [46], but they are limited to solving linear problems and form the basis for more complex neural network models. The architecture of a perceptron closely resembles that of a single-layer feedforward neural network.

### 2.2.3.2    Feedforward Neural Networks

Feedforward Neural Networks (FNNs) (Fig. 2.9) represent the simplest form of neural networks. In this architecture, information flows in a unidirectional manner, starting from the input layer through one or more hidden layers and culminating in the output layer [43]. Each node in a layer is connected to every node in the subsequent layer, with each connection having a weight that influences the signal. Activation functions, such as the sigmoid or ReLU, introduce non-linearity, enabling the network to learn complex relationships. Training involves adjusting these weights based on the error between predictions and actual outputs using optimization algorithms like gradient descent.
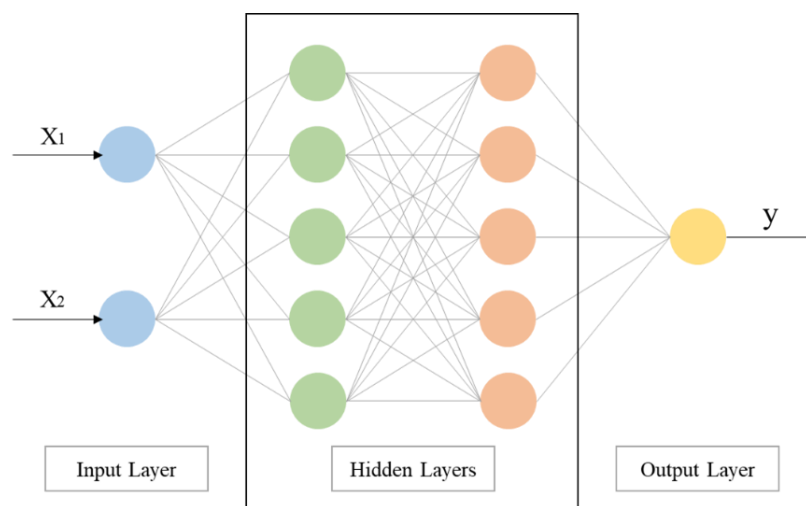


Figure 2.9 Basic Architecture of a Feedforward Neural Network

FNNs serve various applications across different domains. In finance, they are employed for credit scoring and risk assessment [47], [48]. In marketing, FNNs aid in customer segmentation and predicting market trends [49]. Moreover, FNNs find utility in voice and speech recognition systems, contributing to advancements in natural language processing and understanding [50], [51].

### 2.2.3.3   Convolutional Neural Networks

CNNs (Fig. 2.10.) revolutionized image processing tasks. The key feature is the convolutional layer, where filters systematically slide over input data to detect features like edges and textures. Pooling layers reduce spatial dimensions, retaining essential information [52]. Fully connected layers follow, making decisions based on learned features. CNNs leverage parameter sharing and hierarchical feature learning, reducing the number of parameters compared to fully connected networks. This design makes CNNs efficient in image-related tasks by capturing local patterns and spatial hierarchies.
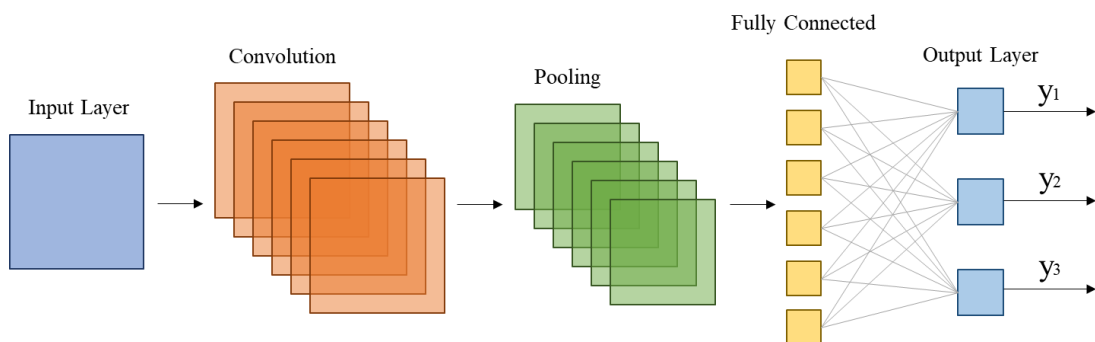
Figure 2.10 Basic Architecture of a Convolutional Neural Network

CNNs have become the foundation of image-related applications. In medical imaging, CNNs are commonly used for tasks such as image classification, object detection, and segmentation of anatomical structures [53], [54]. They have broad applications in facial recognition technology, image-based search engines, and autonomous vehicles for real-time object detection and scene understanding [55], [56].

### 2.2.3.4   Recurrent Neural Networks

Recurrent Neural Networks (RNNs) (Fig. 2.11) are designed for sequential data, such as time series or natural language. Unlike FNNs, RNNs have connections looping back, allowing them to maintain hidden states and capture temporal dependencies [57]. Each step in the sequence processes input alongside information from the previous step.

However, traditional RNNs struggle with vanishing gradients, limiting their ability to capture long-term dependencies [57]. This led to the development of Long Short-Term Memory Networks (LSTMs) and Gated Recurrent Units (GRUs), which address these issues with specialized memory cells and gating mechanisms.
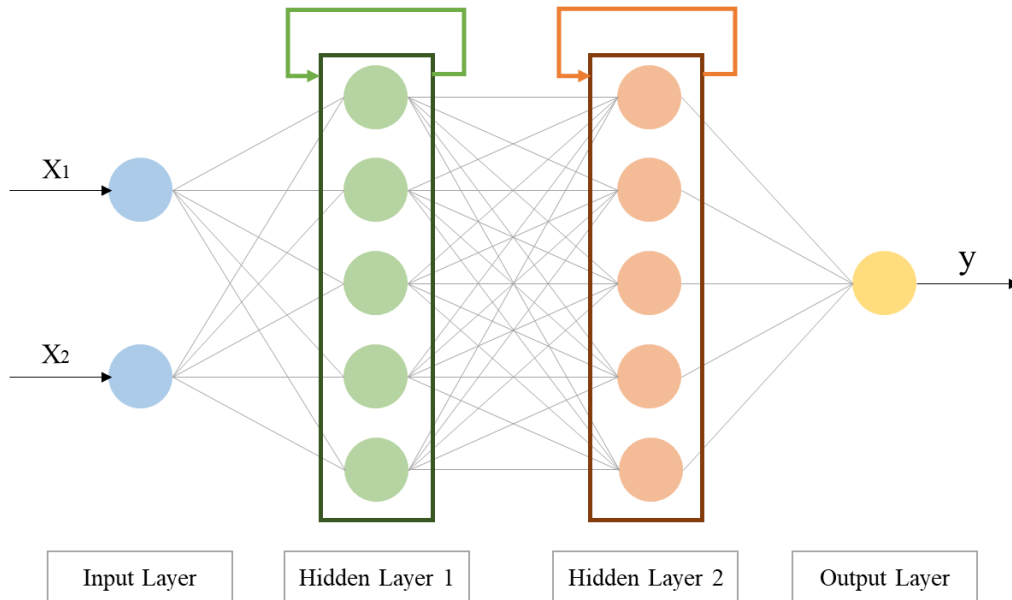


Figure 2.11 Basic Architecture of a Recurrent Neural Network

RNNs are prominently employed in natural language processing applications. In machine translation, RNNs contribute to understanding context and generating coherent translations [58]. In speech recognition systems, RNNs help capture the sequential nature of audio data, enhancing accuracy [59]. Additionally, RNNs find applications in predicting stock prices and analyzing time series data [60].

### 2.2.3.5  Autoencoders

Autoencoders (Fig 2.12) are unsupervised learning models with an encoder-decoder architecture. The encoder compresses input data into a latent representation, and the decoder reconstructs the original data [61]. The model aims to recreate the input accurately, encouraging the learning of efficient representations.
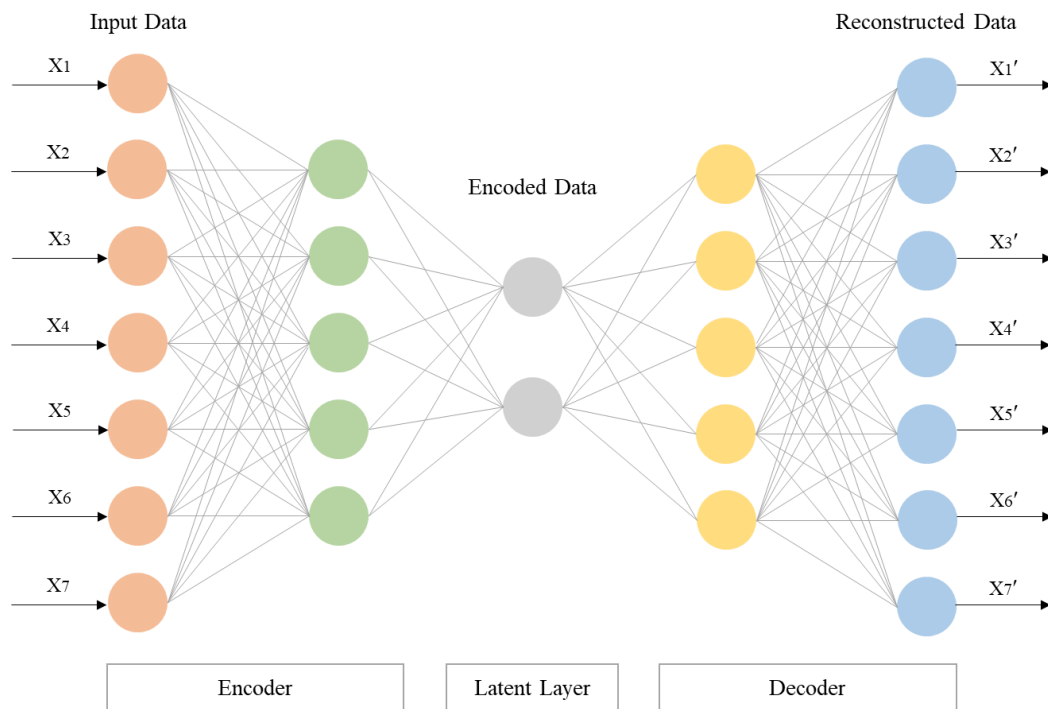
Figure 2.12 Basic Architecture of an Autoencoder

Autoencoders have diverse applications in unsupervised learning scenarios. In anomaly detection, autoencoders identify irregular patterns by learning the normal distribution of data [62]. They are also used in data denoising reconstructing clean data from noisy inputs [63], [64]. Autoencoders contribute to dimensionality reduction in feature learning, aiding in efficiently representing high-dimensional data [65], [66].

### 2.2.3.6 Generative Adversarial Networks

Generative Adversarial Networks (GANs) (Fig. 2.13) consist of a generator and a discriminator engaged in a competitive game. The generator creates synthetic data, and the discriminator evaluates its authenticity [67]. The adversarial process drives both networks to improve iteratively. GANs are powerful in generating realistic data, making them useful in tasks like image synthesis, style transfer, and data augmentation. However, training GANs can be challenging due to their adversarial nature.
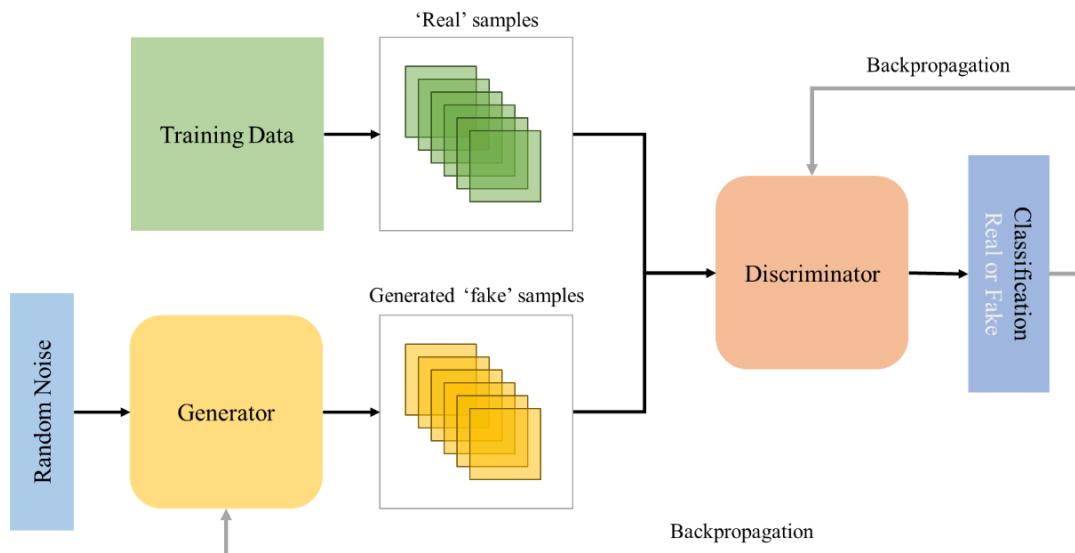
Figure 2.13 Basic Architecture of a Generative Adversarial Network

GANs are primarily known for their applications in image synthesis. In the arts, GANs contribute to creating unique and realistic paintings [68], [69]. In the gaming industry, GANs generate lifelike characters and environments [70], [71]. GANs also play a crucial role in data augmentation, enhancing the diversity of datasets for training robust machine learning models [72], [73].

### 2.2.4   Applications of Neural Networks in Medical Imaging

Neural networks have revolutionized the field of medical imaging, offering unparalleled advancements in the analysis, interpretation, and diagnosis of various medical conditions. By efficiently processing large volumes of imaging data, neural networks enable more accurate and faster diagnoses, enhancing patient care and treatment planning. Their ability to learn from examples and improve over time has made them particularly valuable in identifying patterns and anomalies in complex imaging data that might be indiscernible to the human eye. This capacity for deep learning and pattern recognition is commonly used in areas such as tumor detection [74], [75], organ segmentation [76], [77], and disease progression monitoring [78], [79].

The introduction of CNNs has further transformed medical imaging. CNNs, with their specialized architecture, are great at handling image data, making them ideal for tasks like image classification, segmentation, and enhancement. Their layered structure allows them to automatically and adaptively learn spatial hierarchies of features from

images, leading to more robust and precise interpretations in various medical imaging modalities such as MRI, CT scans, and X-rays. Therefore, CNNs have become an important technology in modern medical imaging, pushing forward the capabilities of automated and accurate medical diagnostics.

## 2.3 Review of 3D CNNs in Alzheimer's Diagnosis

### 2.3.1 Introduction to 3D CNNs

A 3D CNN (Fig. 2.14) represents a sophisticated evolution of the traditional 2D CNN architecture, created specifically to process volumetric data such as 3D images or video sequences. While 2D CNNs excel in spatial feature extraction from images, 3D CNNs extend this capability to three-dimensional structures, making them excellent candidates to perform tasks involving spatial and temporal dimensions [8]. The fundamental unit of a 3D CNN is the 3D convolutional layer, where three-dimensional filters traverse through the entire volume, capturing features across three dimensions. This allows the network to comprehend intricate patterns within volumetric data, which gives an understanding of spatiotemporal relationships.
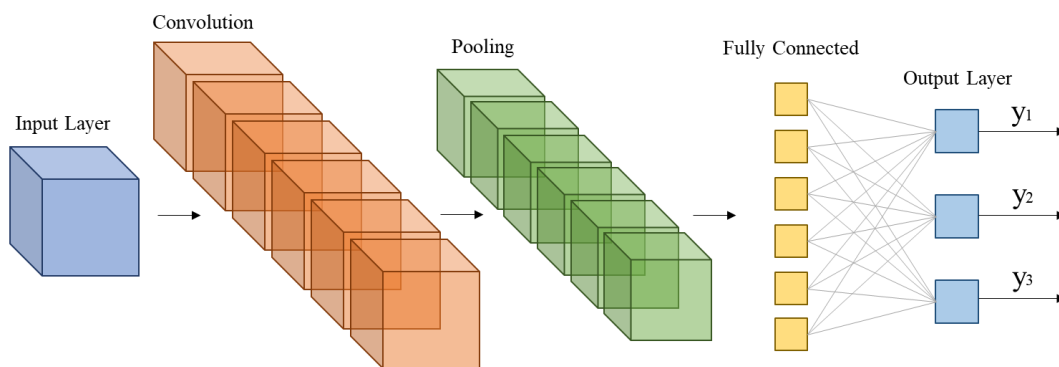


Figure 2.14 Basic Architecture of a 3D Convolutional Neural Network

The distinctive advantage of 3D CNNs lies in their suitability for processing volumetric data. Traditional 2D CNNs may struggle to grasp the complexities of volumetric information, especially in domains like medical imaging [8]. Medical imaging modalities, such as CT or MRI, produce three-dimensional datasets where structures span multiple slices. The 3D convolutional layers in these networks recognize spatial patterns that cover the depth, width, and height of the volumetric data. The improved representations learned by 3D CNNs allow medical professionals to learn about the

complex spatial details of anatomical structures, resulting in more precise and personalized medical interventions.

### 2.3.2　Application of 3D CNNs in Alzheimer's Diagnosis

The application of 3D CNNs in Alzheimer's diagnosis represents a significant advancement in medical imaging technology. Utilizing the detailed spatial information from MRI scans, 3D CNNs are capable of accurately identifying and classifying the various stages of AD [80]. This approach uses the power of deep learning to analyze complex imaging data, offering a promising tool for early detection and better understanding of this neurodegenerative condition. The integration of 3D CNNs in Alzheimer's diagnosis exemplifies the growing impact of artificial intelligence in enhancing diagnostic accuracy and patient care in neurology.

One notable study [81], conducted in 2019, employed a 3D autoencoder model trained on the ADNI dataset. This study achieved an impressive accuracy of 0.93, showcasing the potential of deep learning techniques in accurately diagnosing Alzheimer's disease from MRI scans. Similarly, a study from 2023, referenced by [82], implemented a model comprising 5 convolutional layers and 44 channels, utilizing the ADNI dataset. Although specific preprocessing details were not found, the model achieved a notable accuracy of 0.87, indicating promising results in Alzheimer's disease classification.

In contrast, a study conducted in 2020 [83] utilized the OASIS dataset to train a 3D CNN architecture inspired by VGG-16. Despite employing the same dataset, this model yielded a lower accuracy of 0.69, highlighting the variability in performance observed across different model architectures and datasets. Another study [84] using the OASIS dataset was conducted in 2021. The model achieved an AUC of 0.78, underscoring the importance of comprehensive pre-processing techniques in optimizing model performance.

Furthermore, studies such as the one referenced by [85] in 2019, which utilized 12 repeated blocks of 3D CNNs on the ADNI and Milan datasets, demonstrated exceptional results with an accuracy of 0.98. This study exemplifies the potential of deep learning models, particularly when leveraging complex architectures and diverse datasets.

### 2.3.3  Analysis and Future Directions

The strengths of existing studies in applying 3D CNNs for Alzheimer's diagnosis via MRI data are quite significant. Firstly, many of these studies have showcased high accuracy and specificity in disease detection, which are required for reliable diagnostic tools. This is evidenced by the impressive accuracy rates seen in models like the CBIR and 3D CNN with 12 blocks architectures.

Furthermore, the advanced data processing capabilities of 3D CNNs allow for a detailed analysis of complex brain structures. This aspect is particularly important given the intricate nature of Alzheimer 's-related changes in the brain, which often require precise detection methods. Additionally, the versatility of the architectures used in these studies is notable. The use of various strategies like capsule networks and the incorporation of transfer learning shows the adaptability of 3D CNNs to different datasets and diagnostic requirements.

However, the application of 3D CNNs in Alzheimer's diagnosis faces several challenges and shortcomings:

1. There is a significant dependency on high-quality, large-scale MRI datasets, which are not always available or consistent across different healthcare settings. This variability can impact the accuracy and reliability of the models.
2. The generalizability of these models to diverse populations and clinical environments remains a concern, as they often perform well on specific datasets but may not replicate the same results in different settings.
3. The complexity and computational intensity of 3D CNNs require substantial hardware resources, which may not be feasible in all healthcare institutions, especially in resource-limited areas.

These challenges highlight the need for ongoing research and development to refine and adapt 3D CNNs for broader, more effective use in diagnosing of Alzheimer's disease.

# Chapter 3

# Methodology

## 3.1   Dataset

The use of neural networks for diagnosing Alzheimer's disease has gained significant attention because they can effectively handle complex data. Well-known datasets are available for training and testing neural network models in this area, covering diverse populations, imaging methods, and clinical evaluations. This provides researchers with useful tools for creating precise diagnostic algorithms.

A commonly used dataset for AD diagnosis is the Alzheimer's Disease Neuroimaging Initiative (ADNI) [86]. ADNI is a longitudinal multicenter study that collects extensive neuroimaging, genetic, and clinical data from individuals with AD, MCI, and healthy controls. With its rich dataset that includes structural MRI, fMRI, PET imaging, cerebrospinal fluid biomarkers, and cognitive assessments, ADNI enables researchers to develop neural network models capable of accurately distinguishing between different cognitive states and predicting disease progression.

Another widely utilized resource is the Australian Imaging, Biomarkers & Lifestyle (AIBL) study [87]. AIBL is a longitudinal study focused on identifying biomarkers for

AD using neuroimaging, genetics, and clinical assessments. The dataset includes MRI scans, PET imaging, genetic profiles, and cognitive scores from participants across various cognitive states. By incorporating data from AIBL, researchers can train neural networks to detect subtle changes in brain structure and function indicative of early-stage AD, thus facilitating early diagnosis and intervention.

The European Prevention of Alzheimer's Dementia Consortium (EPAD) is another dataset that offers a significative amount of information about AD, in this case across diverse European populations [88]. This dataset includes neuroimaging data, genetic information, and clinical assessments from multiple European cohorts, enabling researchers to develop neural network models for to different ethnicities and genetic backgrounds. With the help of the EPAD dataset, researchers can explore the heterogeneity of AD presentation and progression, improving the generalizability of diagnostic algorithms.

Other important source is the Open Access Series of Imaging Studies (OASIS) dataset which is the selected dataset for the present study. OASIS offers freely accessible neuroimaging datasets, including MRI and PET scans, from individuals with AD and healthy controls [90]. With its longitudinal design and extensive imaging sequences, OASIS enables researchers to track disease progression over time and develop neural network models capable of accurately diagnosing AD at different stages. Moreover, OASIS and its subsequent versions, such as OASIS 3, plays a key role in advancing our understanding of AD.

The OASIS project began as an initiative to share neuroimaging data related to AD. The project's primary goal was to facilitate research by providing an open platform where researchers could access and analyze structural and functional brain imaging data from individuals with Alzheimer's. The OASIS datasets have been instrumental in the development and validation of various neuroimaging techniques and algorithms for Alzheimer's diagnosis and progression tracking [91], [92].

The OASIS 3 project a part of the Open Access Series of Imaging Studies, contributes valuable data to Alzheimer's research. OASIS 3 includes data from 755 cognitively normal adults and 622 individuals at various stages of cognitive decline, covering a wide age range from 42 to 97 years. This expansive dataset comprises 2,842 MR sessions,

encompassing a variety of sequences such as T1-weighted, T2-weighted, FLAIR, ASL, SWI, TOF, and BOLD.

Many of these MRI sessions are complemented by volumetric segmentation files, processed through Freesurfer, which adds a valuable layer of detail to the data. The dataset includes PET imaging from different tracers totaling over 2,157 raw imaging scans. These scans are accompanied by post-processed files from the PET Unified Pipeline (PUP), further enhancing the dataset's utility for research in Alzheimer's Disease and cognitive aging.

In this study, individual MRI sessions were utilized separately rather than grouped by participant. Specifically, the analysis and findings of the research were solely based on the information derived from the T1-weighted imaging sequence, allowing for a detailed investigation into the structural aspects revealed by MRI scans. The study cohort consisted of individuals aged between 55 and 95 years. The distribution of age, gender, and diagnosis is depicted in Figures 3.1 and 3.2.
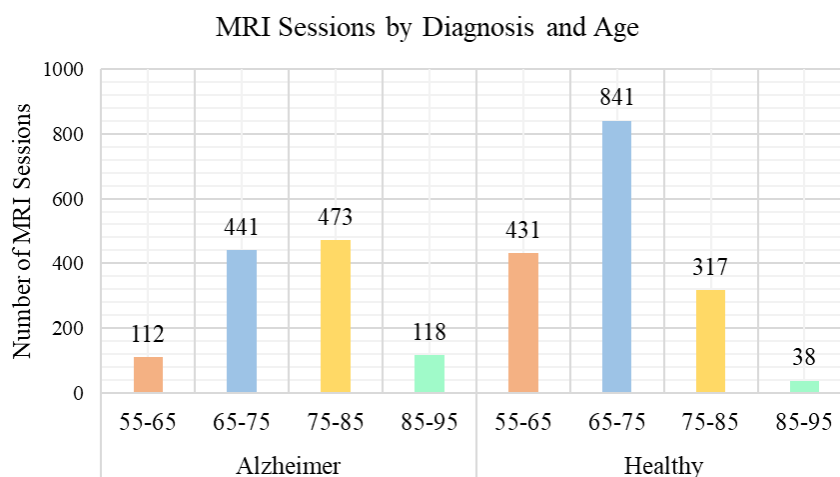


Figure 3.1 Number of T1-weighted MRI Sessions by Age and Diagnosis in OASIS 3 Cohort.
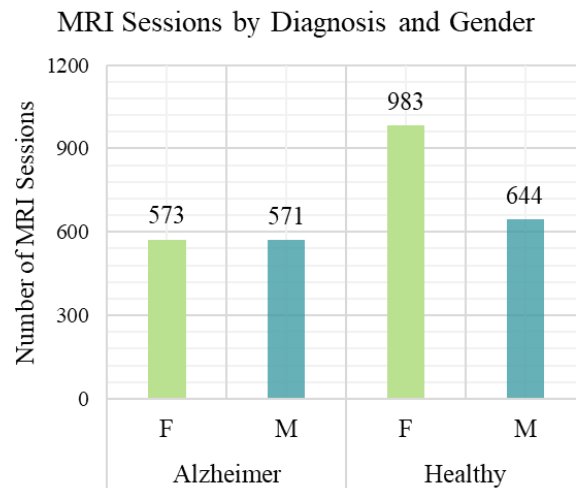
Figure 3.2 Number of T1-weighted MRI Sessions by Gender and Diagnosis in OASIS 3 Cohort.

## 3.2 Pre-processing

The MRI data from the OASIS 3 project hosted on XNAT was downloaded and organized into a structured directory for efficient access during processing. FSL (FMRIB Software Library) was installed within the WSL environment.

FSL is a comprehensive and widely utilized software package in the field of neuroimaging [93]. Developed by the Oxford Centre for Functional MRI of the Brain (FMRIB), FSL was specifically created for the analysis of functional and structural brain imaging data obtained through techniques such as MRI. This robust software suite offers a diverse set of tools and algorithms for tasks such as image pre-processing, registration, segmentation, and statistical analysis. FSL can extract meaningful information from complex neuroimaging datasets, helping researchers and clinicians in understanding the structure and function of the human brain. This open-source software has encouraged collaborative research efforts and has become a fundamental tool in various scientific investigations related to brain health, cognition, and neurological disorders [94], [95].

Before being fed into the neural network, all MRI scans go through a pre-processing pipeline. This pipeline encompasses a series of steps aimed at standardizing and enhancing the quality of the MRI data. The process is illustrated in detail in Figure 3.3, providing a visual representation of the stages within the FSL framework. The initial phase of the pre-processing workflow starts with reorienting the MRI scans to the

standard MNI (Montreal Neurological Institute) axis. This is followed by an automated trimming of the newly oriented images to optimize the image size.
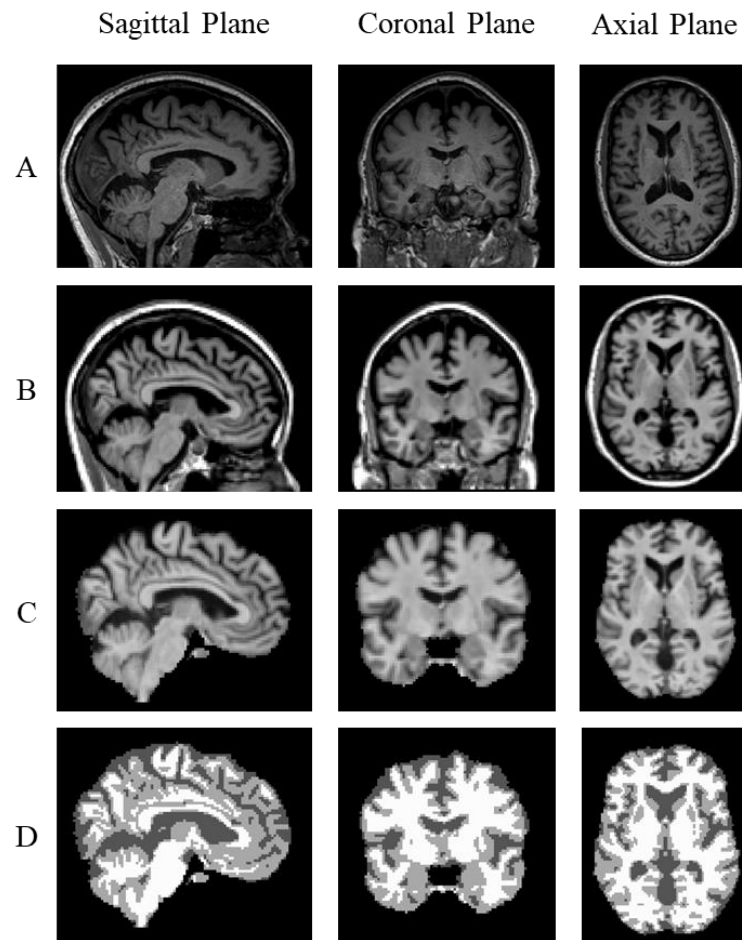


Figure 3.3 FSLeyes visualization of the stages of MRI Image Pre-processing in FSL: A) Original Scan, B) Registration to Standard Space, C) Skull Stripping, D) Tissue-Type Segmentation.

Bias-field correction, an essential procedure to rectify inconsistencies in the magnetic field, known as RF/B1 inhomogeneities, is conducted using the FAST utility. This step is pivotal to normalizing variations in image intensity that could affect analytical accuracy.

The images then undergo a two-stage registration to the standard MNI brain template (Fig. 3.4) to ensure precise anatomical alignment. The FLIRT function facilitates the initial linear registration, setting the foundation for spatial alignment, which is further refined by FNIRT, a tool that fine-tunes the fit via non-linear adjustments. Figure 3.4B shows the brain after registration to a standard.
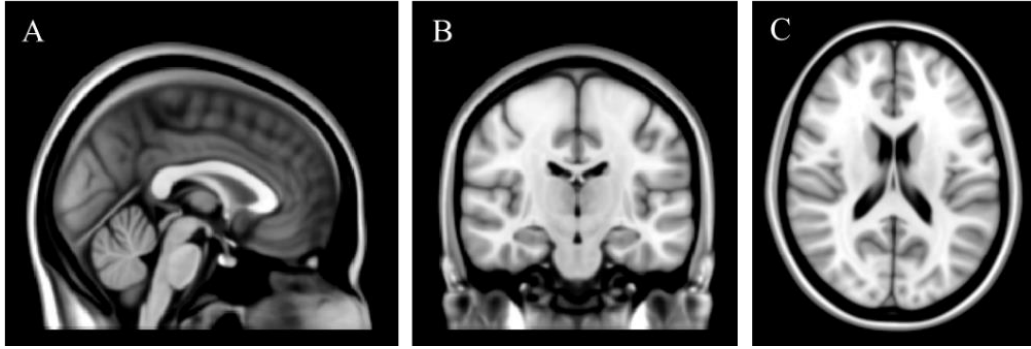
Figure 3.4 FSLeyes visualization of T1-weighted MNI152 template A) Sagittal Plane. B) Coronal Plane. C) Axial Plane.

The BET command, also part of FSL, is applied next to extract the brain from surrounding tissue (Fig. 3.2C), a step critical for isolating the area of interest. Subsequently, the FAST function segments the brain tissue (Fig. 3.2D) into gray matter (GM), white matter (WM), and CSF, allowing for detailed tissue analysis.

Integral to the pre-processing is a stringent quality control process. This involves meticulous inspection of the images post-processing to validate the precision of each step. Tools like FSLeyes are instrumental in this phase, offering a visual interface for reviewing and confirming the quality and accuracy of the pre-processing workflow.

Following the completion of Tissue-Type Segmentation in FSL, the segmented data is uploaded to Google Colab to take advantage of its GPU processing capabilities and drive storage access. The initial step in the code involves loading demographic and diagnostic information from an Excel file. Subsequently, the data is split into training, validation, and test sets, ensuring a balanced distribution of diagnostic classes. To address potential class imbalances, class weights are computed based on the training set. Mathematically the class weight for each class $c_i$ is calculated with the equation 3.1.

$$w_{c_i} = \frac{n_{samples}}{n_{classes} \times n_{c_i}} \tag{3.1}$$

## 3.3   Data Generation and Augmentation

A Data Generator is used to facilitate batch-wise feeding of the neural network during training. This generator handles data loading, balancing, and augmentation, providing the necessary inputs and corresponding labels for the model. The functions used during data generation are data loading, channel separation, and augmentation.

Three instances of the data generation are used as training, validation, and test generators. The training set generator includes an option for data augmentation, while the validation and test sets remain unaltered. These generators will be employed to feed data to the 3D CNN model during the training and evaluation phases. The data generator encapsulates a comprehensive data preparation pipeline, ensuring the model receives appropriately formatted and balanced input data for effective learning and evaluation.

### 3.3.1    Data loading and 3-channel Representation

The neuroimaging data in NIfTI format is loaded and processed, creating a 3-channel representation for each voxel (Fig. 3.5).
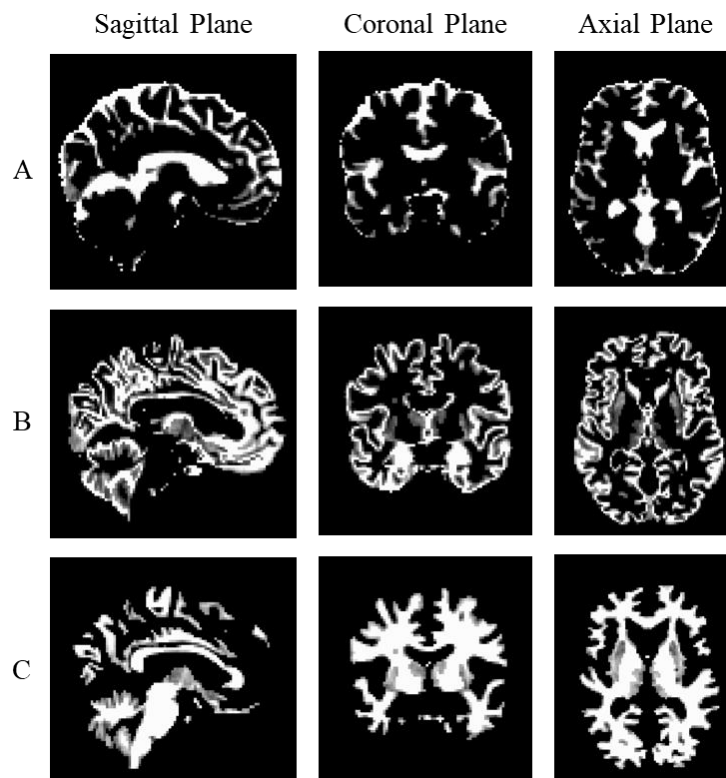


Figure 3.5 Post-Segmentation MRI Tissue Classification: A) CSF Channel, B) GM Channel, C) WM Channel

This representation is achieved by utilizing a mathematical formulation where each voxel in the segmented image is encoded across three channels, corresponding to the presence or absence of each class label. Mathematically, this can be expressed as follows:

Let $n$ represent the total number of voxels in the segmented image.

For each voxel $v_i$ in the segmented image:

$$v_i = (x_{i1}, x_{i2}, x_{i3}) \qquad (3.2)$$

Where $x_{i1}, x_{i2}$ and $x_{i3}$ represent the presence (1) or absence (0) of the voxel belonging to class labels 1, 2 and 3, respectively.

The 3-channel representation for each voxel can be created using the formula:

$$\text{Channel}_j(v_i) = \begin{cases} 1 \text{ if the voxel belongs to class } j \\ \qquad 0 \text{ otherwise} \end{cases} \qquad (3.3)$$

For $j = 1, 2, 3$.

### 3.3.2   Data Augmentation

The augmentation is implemented to artificially increase the dataset size through transformations. The scaling and flipping functions effectively change the original image, resulting in either of these transformations as the augmented image.

### 3.3.2.1   Scaling

Scaling the image involves multiplying the spatial coordinates of each voxel in the image that we have after the channel separation by a specified scale factor $s$. Mathematically, the scaled image $I'$ is obtained by:

$$I'(x, y, z, c) = I(sx, sy, sz, c) \qquad (3.4)$$

where $x, y, z$ represent the spatial dimensions of the image, and c represents the channel index.

Next, the excess size resulting from the scaling operation is then calculated by subtracting the original size of the image from the size of the scaled image in each dimension. For each dimension $d$ (width, height, depth), the excess size $E_d$ is given by:

$$E_d = I'_{size_d} - I_{size_d} \qquad (3.5)$$

To obtain the final augmented image, the excess regions resulting from scaling are trimmed, and the remaining central region is retained to match the original size. The start index $S_d$ for cropping in each dimension $d$ is calculated as half of the excess size:

$$S_d = \frac{E_d}{2} \qquad (3.6)$$

The end index $E'_d$ for cropping in each dimension $d$ is then calculated by adding the start index to the original size of the image in that dimension:

$$E'_d = S_d + I_{size_d} \tag{3.7}$$

Finally, the augmented image $I_{augmented}$ is obtained by cropping the scaled image to the original size using the calculated start and end indices in each dimension:

$$I_{augmented}(x, y, z, c) = I'(x', y'z', c) \tag{3.8}$$

This process ensures that the image is scaled while preserving its original size, and any excess regions resulting from scaling are trimmed to maintain the original dimensions.

### 3.3.2.2  Flipping

The flip transformation is performed along the axis 0, if $D$ represents the image and $D'$ represents the augmented image obtained after the operation, then foreach voxel $(x, y, z)$ in the original image:

$$D'(x', y', z', c) = D(x, -y, z, c) \tag{3.9}$$

Here, $(x', y', z')$ are the coordinates of the corresponding voxel in the augmented image, where $x'$ and $z'$ remain unchanged and $y'$ is flipped to its negative value $(-y)$

### 3.4   3D CNN Architecture and Design

This CNN model is designed for 3D image classification, taking input volumes of shape (91, 109, 91, 3), where 91x109x91 represents the spatial dimensions of the 3D image, and 3 denotes the number of channels. The model architecture consists of multiple layers to extract features and classify the input into one of two classes, making it suitable for binary classification tasks (Fig. 3.6).
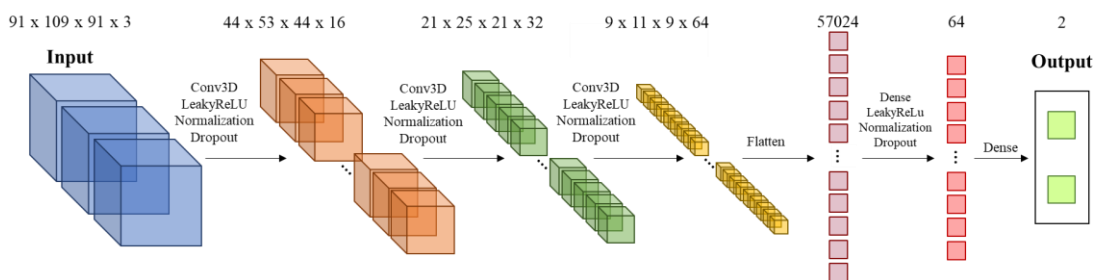


Figure 3.6. Architecture and design of the proposed 3D CNN Model

The input volume passes through a series of Conv3D layers, each performing 3D convolutions to extract spatial features from the input data. These convolutional layers are followed by LeakyReLU activation functions, which introduce non-linearity to the model. Batch normalization layers are applied after activation to normalize the activations and accelerate the training process.

Max-pooling layers with a pool size of (2, 2, 2) are utilized to down sample the spatial dimensions of the feature maps, reducing computational complexity while retaining important features. Dropout layers with a dropout rate of 0.25 are inserted after each max-pooling layer to prevent overfitting by randomly dropping a fraction of input units during training.

After the feature extraction process, the 3D feature maps are flattened into a 1D vector using a Flatten layer, enabling the transition to fully connected dense layers. Two dense layers with 64 neurons each are employed for further feature refinement and abstraction. LeakyReLU activation functions, batch normalization, and dropout (with a rate of 0.5 for the last dropout layer) are applied to these dense layers to enhance model generalization and prevent overfitting.

Finally, the output layer consists of a single dense layer with 2 neurons and a sigmoid activation function. This sigmoid activation function squashes the output between 0 and 1, enabling binary classification. The output neuron values represent the model's confidence scores for each class, and a threshold (typically 0.5) is applied to assign the input volume to one of the two classes based on whether the output is above or below the threshold. Thus, the model effectively converts the input 3D image volume into a binary classification decision.

### 3.4.1 Conv3D Layer

The Conv3D operation in neural networks, also known as 3D convolution, is a fundamental operation used for extracting features from volumetric data such as video, medical imaging, or 3D spatial data.

Mathematically, let's consider a 3D input tensor $X$ with shape $(D, H, W, C_{in})$ where $D$ is the depth or number of slices, $H$ is the height or number of rows, $W$ is the width or number of columns, and $C_{in}$ is the number of input channels.

For simplicity, let's consider a single convolutional filter (or kernel) $K$ with shape ($d_k$, $h_k$, $w_k$, $C_{in}$, $C_{out}$), where $C_{out}$ is the number of output channels.

The Conv3D operation involves sliding the convolutional filter $K$ across the input tensor $X$ and computing the element-wise multiplication between the filter and the corresponding input patch, followed by summing the results. This process is performed independently for each output channel.

Mathematically, the Conv3D operation can be represented as:

$$Y_{i,j,k,c} = \sum_{d=0}^{d_k-1} \sum_{r=0}^{h_k-1} \sum_{s=0}^{w_k-1} \sum_{m=0}^{C_{in}-1} X_{i+d,j+r,k+s,m} \times K_{d,r,s,m,c} \qquad (3.10)$$

Where:

- $Y_{i,j,k,c}$ represents the value of the output tensor at position $(i,j,k,c)$
- $X_{i+d,j+r,k+s,m}$ represents the value of the input tensor at position $(i+d,j+r,k+s,m)$
- $K_{d,r,s,m,c}$ represents the value of the convolutional filter at position $(d,r,s,m,c)$

The convolutional filter $K$ is applied to every possible position in the input tensor $X$ along the spatial dimensions (depth, height, width), and for each position, the element-wise multiplication and summation are performed to compute the corresponding output value.

This operation results in an output tensor $Y$ with shape ($D_{out}$, $H_{out}$, $W_{out}$, $C_{out}$), where $D_{out}$, $H_{out}$, $W_{out}$, represent the dimensions of the output tensor, and $C_{out}$ represents the number of output channels.

The Conv3D operation performs a 3D convolutional operation on the input tensor X using a set of learnable convolutional filters K to extract features and produce an output tensor Y.

### 3.4.2 LeakyReLU Activation

The LeakyReLU activation function introduces a small slope for negative inputs, denoted by the parameter $\alpha$, ensuring a non-zero output even when the input is negative. Mathematically, for any given input $x$, LeakyReLU computes the output as follows:

$$f(x) = \begin{cases} \alpha x & if \ x < 0 \\ x & if \ x \geq 0 \end{cases} \qquad (3.11)$$

In this formulation, when x is negative, the output is $\alpha$ times $x$, where $\alpha$ is typically set to a small positive value such as 0.01 or 0.1. This ensures that even for negative inputs, a fraction of the information is preserved, allowing gradients to flow during backpropagation and preventing the issue of neurons becoming "dead" or inactive.

By incorporating this small slope for negative inputs, LeakyReLU addresses the limitations of traditional ReLU activation, enabling networks to learn more robust features and improving the overall training dynamics. Because the function behaves identically to ReLU for non-negative inputs, it retains the computational efficiency and simplicity associated with ReLU while mitigating its drawbacks.

### 3.4.3 Batch Normalization

Batch normalization (BatchNorm) is a technique that significantly enhances training stability and convergence rates. It addresses the issue of internal covariate shift by normalizing the activations of each layer within the neural network.

The process begins with the input activations, denoted as $x$, which represent the output of a layer. BatchNorm then standardizes these activations by subtracting the mean ($\mu$) and dividing by the standard deviation ($\sigma$) calculated over a mini-batch of data. This normalization step ensures that the input to each layer has a consistent distribution, regardless of variations in the input data. Mathematically, the normalized activations are computed as:

$$BatchNorm(x) = \frac{x-\mu}{\sqrt{\sigma^2+\epsilon}} \times \gamma + \beta \qquad (3.12)$$

Here, $\epsilon$ is a small constant added for numerical stability to prevent division by zero. Additionally, $\gamma$ and $\beta$ are learnable parameters that allow the model to scale and shift the normalized activations, respectively. These parameters are updated during training via backpropagation, allowing the model to adapt to the data distribution and optimization process.

Batch normalization confers several benefits to the training process. First and foremost, it mitigates the vanishing/exploding gradient problem by ensuring that the input activations are maintained within a reasonable range. This leads to more stable gradients and accelerates convergence during training. Furthermore, by reducing the internal

covariate shift, batch normalization acts as a form of regularization, reducing the risk of overfitting and improving the generalization performance of the model.

During inference, batch normalization ensures that the model behaves consistently across different mini-batches or input data sizes. This is achieved by computing the mean and standard deviation based on the entire dataset or using moving averages of mini-batch statistics collected during training. Consequently, the model produces reliable predictions regardless of the input data distribution.

### 3.4.4  Max Pooling Layer

MaxPooling3D is a key operation in 3D convolutional neural networks (CNNs) for down sampling input volumes while retaining critical features. It involves dividing the input volume into non-overlapping regions and selecting the maximum value within each region. Mathematically, if we denote the input volume as $V_{in}$, the operation of MaxPooling3D can be represented as follows:

$$V_{\text{out}} = max_{a,b,d} V_{in}(2i + a, 2j + b, 2k + d, c) \tag{3.13}$$

where $V_{\text{out}}(i, j, k, c)$ represents the output volume at position $(i, j, k)$ of channel $c$, and $a$, $b$, $d$ iterate over the pooling window size (e.g., 2x2x2).

This operation effectively reduces the spatial dimensions of the input volume by a factor determined by the pooling window size, while preserving the most salient features. By summarizing local information and discarding less relevant details, MaxPooling3D enhances the network's ability to capture high-level patterns and structures within volumetric data.

The layer MaxPooling3D helps improve computational efficiency by reducing the number of parameters and computations required in subsequent layers. Additionally, it facilitates translation invariance, allowing the network to recognize features regardless of their precise spatial location within the input volume.

### 3.4.5  Dropout Layer

Dropout is a regularization technique used in neural networks during training to prevent overfitting. It works by randomly deactivating a fraction of neurons with a probability defined by the dropout rate. Mathematically, dropout can be represented as:

$$Output = Input \times Mask \tag{3.14}$$

*Input* represents the activations of a layer before dropout and *Mask* is a binary mask with the same shape as the input, where each element is randomly set to 0 or 1 with a probability defined by the dropout rate.

During training, each element in the mask is independently set to 0 with a probability equal to the dropout rate, and to 1 otherwise. The activations are then multiplied element-wise by the mask. This process effectively deactivates a fraction of neurons, forcing the network to learn more robust features that are not overly dependent on specific neurons.

By randomly deactivating neurons, dropout introduces noise into the network and prevents co-adaptation of neurons, improving the model's generalization performance. During inference, dropout is typically turned off, and the activations are scaled by the inverse of the dropout rate to ensure consistent behavior.

### 3.4.6   Flatten Function

The "flatten" operation in neural networks is a simple reshaping operation that transforms multi-dimensional input into a one-dimensional array.

Mathematically, let's say we have a multi-dimensional tensor $X$ of shape $(n_1, n_2, \ldots, n_k)$. After applying the "flatten" operation, the resulting one-dimensional array $X'$ is obtained by concatenating all the elements of $X$ along a single dimension.

If $X$ is a tensor of shape $(n_1, n_2, \ldots, n_k)$, then $X'$ will be a vector of length $n_1 \times n_2 \times \ldots \times n_k$.

In other words, the "flatten" operation preserves the order of elements in the original tensor but rearranges them into a one-dimensional sequence.

Mathematically, the "flatten" operation can be represented as follows:

$$X' = [X[\,1, 1, \ldots, 1], X[1, 1, \ldots, 2], \ldots, X[n_1, n_2, \ldots, n_k]] \tag{3.15}$$

Here $X[i_1, i_2, \ldots, i_k]$ represents the elements of tensor $X$ at position $(i_1, i_2, \ldots, i_k)$

This operation is commonly used in neural networks to transition from convolutional or recurrent layers, which typically work with multi-dimensional data, to fully connected

(dense) layers, which require one-dimensional input. It allows the network to flatten the spatial or temporal dimensions of the data and feed it into a dense layer for further processing.

### 3.4.7   Dense Layer

The dense layer, a core component in neural networks, operates by computing the output based on the input, weights, and biases, and applying an activation function to the resulting linear combination.

Mathematically, the Output of the dense layer is represented as:

$$\text{Output} = \text{Activation}(W \cdot \text{Input} + b) \tag{3.16}$$

Here, Input denotes the input to the dense layer, $W$ represents the weight matrix, and $b$ is the bias vector. The weight matrix $W$ dictates the contribution of each input feature to the output and has dimensions ($n_{curr}$, $n_{prev}$), where $n_{curr}$ is the number of neurons in the current layer and $n_{prev}$ is the number of neurons in the previous layer. Each element $W_{ij}$ in the weight matrix represents the weight connecting neuron $i$ in the current layer to neuron $j$ in the previous layer. The bias vector $b$ provides each neuron with an additional parameter to control its output and has dimensions ($n_{curr}$,1), where each element $b_i$ represents the bias term associated with neuron $i$ in the current layer.

In the context of regularization techniques, a kernel regularizer can be applied to the dense layer to control the complexity of the model and prevent overfitting. One commonly used regularizer is $L_2$ regularization, which penalizes large weights in the dense layer. Mathematically, the $L_2$ regularization term is represented as:

$$\text{Regularization Term} = \frac{\lambda}{2}\sum_{i,j} W_{ij}^2 \tag{3.17}$$

Here, $\lambda$ is the regularization factor, and $W_{ij}$ denotes individual weights in the weight matrix $W$.

Besides $L_2$ regularization, there are other regularization techniques such as $L_1$ regularization, which penalizes the absolute values of the weights, and dropout, which randomly drops a fraction of neurons during training to prevent overfitting.

On the other hand, setting the activation function to 'sigmoid' in the dense layer constrains the output of each neuron to the range [0, 1]. The sigmoid function transforms the linear combination of inputs and biases into a probability-like output suitable for binary classification tasks. Mathematically, the sigmoid activation function is represented as:

$$\sigma(x) = \frac{1}{1+e^{-x}} \tag{3.18}$$

Here, $x$ represents the input to the activation function.

In summary, the dense layer computes its output based on the input, weights, and biases, and applies an activation function to introduce non-linearity. Regularization techniques such as $L_2$ regularization can be applied to control the complexity of the model, while choosing appropriate activation functions like 'sigmoid' helps in achieving specific task objectives, such as binary classification. These mechanisms contribute to the overall performance and robustness of the neural network, enhancing its ability to generalize well to unseen data.

## 3.5   Training and Validation

The implementation of training and validation procedures incorporates an Early Stopping callback, a technique to monitor the validation loss during training and halt the process if there is no improvement for a specified number of epochs (patience). This is a preventive measure against potential overfitting, and the restore best weights parameter is used to ensure that the model reverts to the weights that resulted in the lowest validation loss.

The actual model training is executed using the 'fit' function. The generator provides the training data, an instance of the data generation, which facilitates batch-wise data feeding during training. The number of steps per epoch and validation steps are carefully calculated based on the size of the datasets and the chosen batch size considering the augmentation.

The class weight parameter is set to address potential class imbalances in the training data. This is particularly important when dealing with datasets where certain classes may be underrepresented. In this case, the number of healthy patients is more significant than those with AD.

## 3.6   Evaluation Metrics

The following plots and calculations offer a thorough analysis of the 3D CNN model's performance. The choice of these metrics and visualizations ensures a comprehensive evaluation across different aspects of classification. They collectively offer a detailed understanding of the model's strengths and weaknesses, aiding in the interpretation and fine-tuning of the neural network for optimal results.

### 3.6.1   Loss and Accuracy Plots

During the training process, the model generates visual representations illustrating both training and validation loss and accuracy over each epoch. These plots are critical for evaluating the model's learning trajectory and ability to apply that learning to new, unseen data.

Training loss, calculated using a loss function $L_{train}$, quantifies the error between the model's predictions $\hat{y}$ and the actual data $y$, with a downward trend indicating improvement. Mathematically, it can be represented as:

$$L_{train} = \frac{1}{N}\sum_{i=1}^{N} \text{loss}(\hat{y}_i, y_i) \tag{3.19}$$

where $N$ is the number of training samples, $\hat{y}_i$ is the predicted output for the $i$-th sample, $y_i$ is the true label for the $i$-th sample, and $\text{loss}(\cdot)$ is the chosen loss function.

Training accuracy, denoted as $Acc_{train}$, reflects the percentage of correct predictions made on the training data. It is calculated as the ratio of the number of correctly predicted samples to the total number of training samples. Mathematically, it can be represented as:

$$Acc_{train} = \frac{Number\ of\ correctly\ predicted\ samples}{Total\ number\ of\ training\ samples} \times 100\% \tag{3.20}$$

Conversely, validation loss $L_{val}$ and validation accuracy $Acc_{val}$ measure the model's error and predictive performance on a separate set of data not used during training. Validation loss and accuracy are calculated similarly to training loss and accuracy but using the validation data set. These metrics provide a gauge for the model's generalization ability, indicating how well the model performs on unseen data.

### 3.6.2    Classification Metrics and Confusion Matrix

The model calculates key classification metrics, including accuracy, precision, recall, and the F1 score [96]. These metrics provide helpful information about the model's performance and its ability to effectively classify instances.

Accuracy (Acc) represents the ratio of correctly predicted instances to the total predictions made. Mathematically, it can be calculated as:

$$Acc = \frac{TP+TN}{TP+TN+FP+FN} \tag{3.21}$$

Precision (Prec) is the proportion of true positive predictions out of all positive predictions made, indicating the model's specificity. It is calculated as:

$$Prec = \frac{TP}{TP+FP} \tag{3.22}$$

Sensitivity (Sens), recall or True Positive Rate, measures the proportion of actual positives that were correctly identified. It is calculated as:

$$Sens = \frac{TP}{TP+FN} \tag{3.23}$$

Specificity (Spec) or True Negative Rate represents the proportion of actual negatives that were correctly identified and is calculated as:

$$Spec = \frac{TN}{TN+FP} \tag{3.24}$$

The F1 score is the harmonic mean of precision and recall, providing a balance between them. It is calculated as:

$$F1 = \frac{2 \times Prec \times Sens}{Prec+Sens} \tag{3.25}$$

The confusion matrix is a tabular visualization that delineates the correct and incorrect predictions across different classes. It consists of four metrics: True Positives (TP), True Negatives (TN), False Positives (FP), and False Negatives (FN). These metrics clarify where the model excels or falters in its predictions.

These metrics collectively offer a nuanced view of the model's classification prowess, aiding in evaluating its performance and identifying areas for improvement.

### 3.6.3   ROC curve and AUC

The Receiver Operating Characteristic (ROC) curve is a plot that evaluates the model's performance across various classification thresholds, showing the trade-off between sensitivity (true positive rate) and specificity (false positive rate) [96]. It is calculated by plotting the true positive rate against the false positive rate at different threshold settings. The Area Under the Curve (AUC) is a single scalar value summarizing the curve, with a higher AUC indicating a model's better discrimination between classes [96].

### 3.6.4   Precision-Recall Curve and Average Precision

In the context of imbalanced classes, the Precision-Recall curve is particularly informative. It plots the precision (the accuracy of positive predictions) and recall (the ability to find all positive samples) for different threshold values [96]. The Average Precision (AP) score integrates the precision-recall curve to provide an overall effectiveness measure of positive predictions, especially useful when classes are imbalanced.

The AP score reflects the weighted mean of precision achieved at each threshold, emphasizing the contribution of high-recall thresholds. It is calculated by computing the area under the precision-recall curve using methods such as numerical integration or the trapezoidal rule.

$$AP \ = \ \sum_k (R_k - R_{k-1}) \times P_k \tag{3.26}$$

Where $R_k$ and $P_k$ represent recall and precision at each threshold, respectively, and the sum is taken over all thresholds. Overall, the Precision-Recall curve and AP score provide valuable insights into the model's performance, particularly in scenarios with imbalanced class distributions.

# Chapter 4

# Results and Discussion

## 4.1   Model Performance

The 3D CNN model underwent a 30-epoch training process, culminating in impressive performance metrics. Upon completion of training, the model achieved a training accuracy of 93.03% with corresponding precision, recall, and AUC values of 92.51%, 92.21%, and 97.80%, respectively. During validation, the model demonstrated robustness with an accuracy of 88.05%, precision of 87.50%, recall of 87.50%, and an AUC of 93.7% at epoch 30. Testing the model on an independent dataset resulted in an impressive accuracy of 91.01%, precision of 90.18%, recall of 87.83%, and an F1 score of 88.99%. The confusion matrix highlighted the model's ability to accurately classify instances, with 152 true negatives, 101 true positives, 11 false positives, and 14 false negatives. These outcomes collectively affirm the model's proficiency in discerning between classes and underscore its potential for meaningful clinical applications in the diagnosis of the targeted condition.

## 4.2   Evaluation Metrics Analysis

The evaluation metrics analysis begins by examining the progression of performance metrics across epochs during the training and validation of the 3D CNN model, as

depicted in Figure 4.1. The training accuracy consistently increased, reaching a peak of 93.03% by epoch 30, showing the model's ability to progressively learn from the training data. Concurrently, precision and recall values for the training set demonstrated a consistent upward trend, showing the model's improved capacity to correctly identify positive instances while minimizing false positives. The AUC metric, an indicator of overall model performance, steadily rose to an impressive 97.80% after training. In the validation phase, the model exhibited good generalization capabilities, achieving an accuracy of 88.05%, precision and recall both at 87.50% and an AUC of 93.7% at epoch 30. These trends collectively suggest that the model not only is good in learning from the training data but also performs robustly on unseen validation data, substantiating its potential for practical application in real-world scenarios.
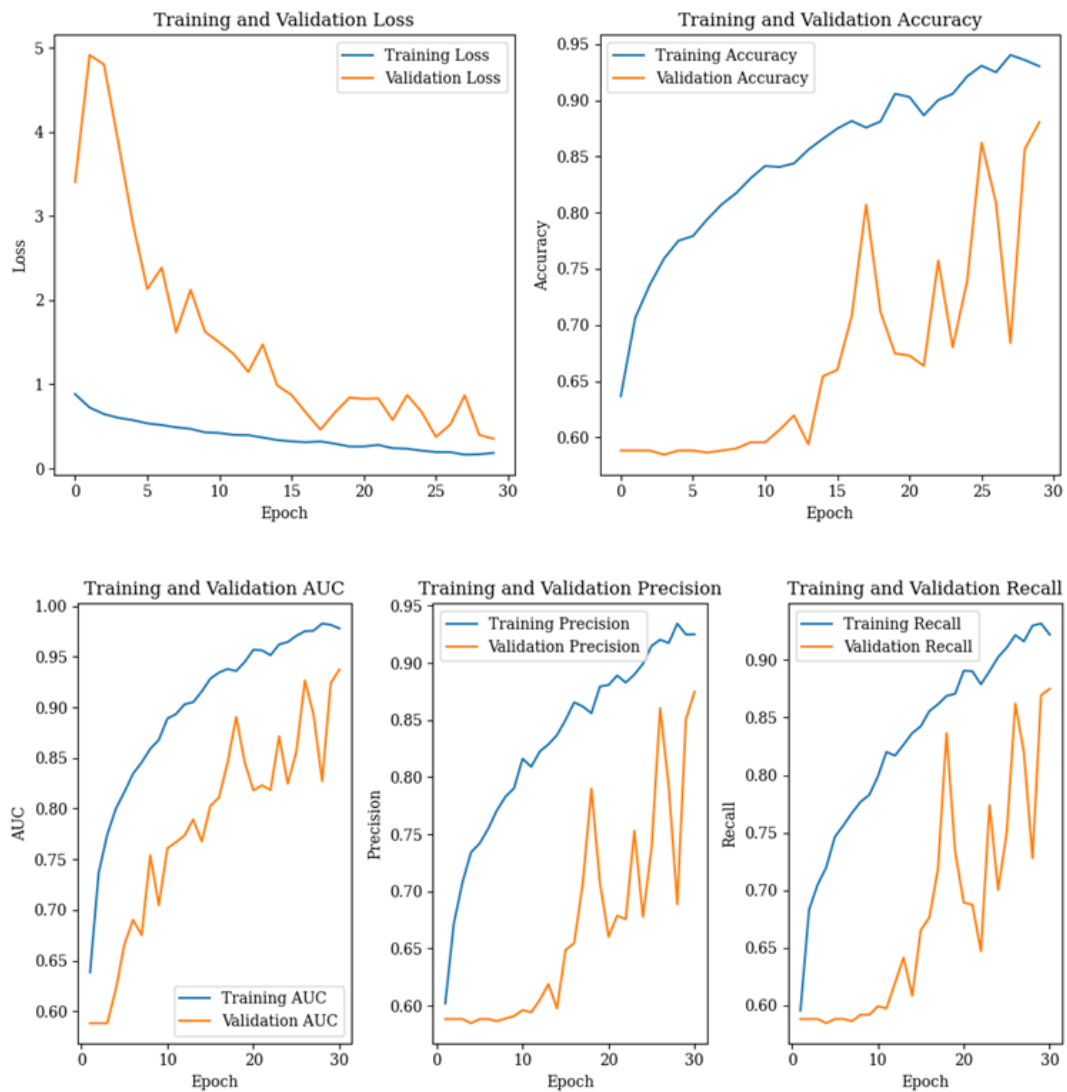


Figure 4.1 Performance Metrics Over Epochs for the Proposed Model: Training and Validation Loss, Accuracy, AUC, Precision, and Recall.

In evaluating the model's performance on the test set, the conventional threshold of 0.5, a standard choice for binary classification, is first considered. The results at this threshold reveal a commendable accuracy of 91%, indicating the proportion of correctly classified instances among the total. Precision, representing the positive predictive value, is high at 90%, implying that when the model predicts an individual as having Alzheimer's disease, it is accurate 90% of the time. The recall, or sensitivity, is 87.8%, signifying the model's ability to identify the majority of actual positive cases. The F1 score, balancing precision and recall, is 88.99%.

Now, with a lowered threshold of 0.2, there are changes in the model's behavior. This adjustment is often needed+ in medical contexts, where minimizing false negatives (missed cases) is critical. The test accuracy remains high at 91%, but the recall increases to 87.8%, suggesting a reduction in missed positive cases. However, the precision decreases to 90.18%, indicating a higher rate of false positives. The F1 score remains at 88.99%. Examining the confusion matrix (Fig. 4.2), we observe a trade-off: a decrease in false negatives (14 to 2) and an increase in false positives (11 to 24).
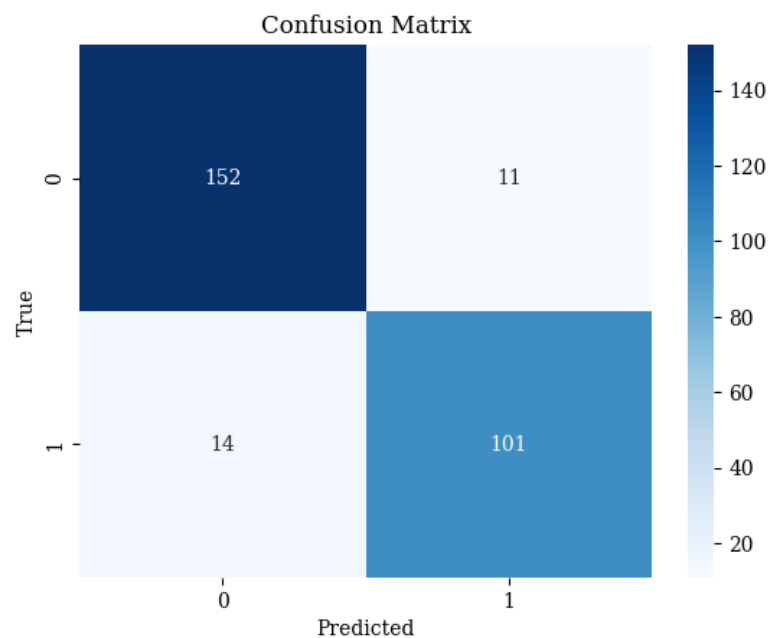


Figure 4.2 Binary Classification Confusion Matrix Visualization

An area under the ROC curve (AUC-ROC) and an area under the precision-recall curve (AUC-PR) of 0.96 suggests that the model has achieved high discriminative performance on the test set. The ROC curve (Fig. 4.3) represents the trade-off between true positive rate (sensitivity) and false positive rate. In contrast, the precision-recall curve focuses on

precision (positive predictive value) and recall (sensitivity). In both cases, an AUC of 0.96 indicates excellent model performance, showcasing its ability to distinguish between different classes. This implies that the model's predictions align well with the ground truth labels, achieving a balance between identifying positive instances and minimizing false positives. Such high AUC values are indicative of a robust and reliable model, providing confidence in its effectiveness for the given classification task.
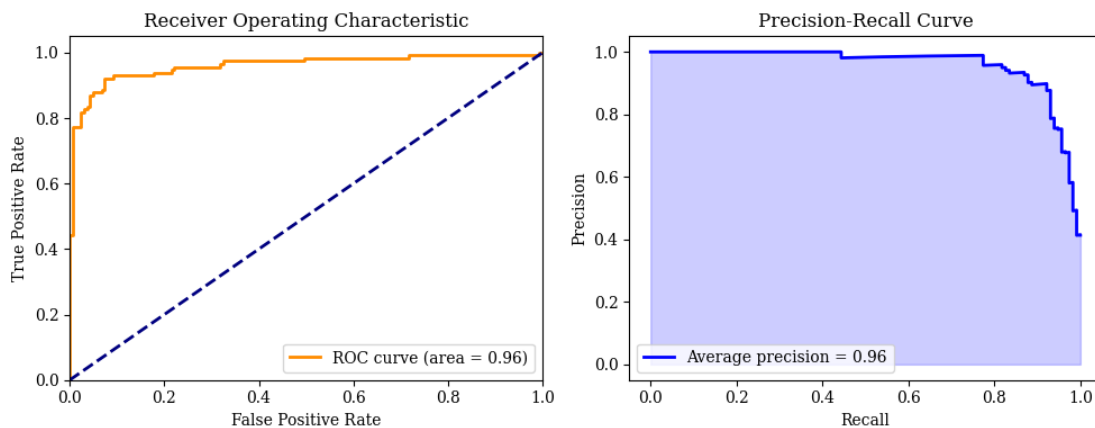


Figure 4.3 ROC and Precision-Recall Curves Demonstrating Model Performance Metrics

## 4.3    Limitations

### 4.3.1    Dataset Limitations

The dataset used in this project, derived from the OASIS 3 database, presents several limitations that warrant consideration. Firstly, the dataset exhibits class imbalance between healthy controls and individuals diagnosed with Alzheimer's disease. Such an imbalance may introduce bias during model training and evaluation, potentially leading to overestimation of the model's performance on the majority class while neglecting the minority class. Moreover, the OASIS 3 dataset, while widely utilized in Alzheimer's disease research, may lack diversity in terms of demographic characteristics, imaging protocols, and disease progression stages. This limited diversity can restrict the generalizability of findings, as the model may not effectively capture the heterogeneity present in broader populations. Additionally, the dataset is confined to T1-weighted MRI scans, overlooking potentially valuable information available in other modalities such as T2-weighted MRI or diffusion-weighted imaging. Consequently, the reliance on a single modality may limit the model's ability to extract comprehensive features relevant to Alzheimer's disease classification.

### 4.3.2   Preprocessing Limitations

The preprocessing steps applied to the dataset before model training also entail certain limitations that necessitate scrutiny. Firstly, while utilizing FSL for brain segmentation is a common practice, it's crucial to recognize the potential for segmentation inaccuracies. The precision of this segmentation directly impacts the quality of the extracted features used for classification. Inaccurate segmentation may introduce noise or distortions into the data, compromising the model's ability to discern meaningful patterns. Additionally, although data augmentation techniques such as flipping or scaling were employed to enhance the diversity of the training dataset, it's essential to acknowledge the inherent trade-offs associated with these methods. While augmentation can effectively increase the variety of samples available for training, it may also introduce artificial patterns or distortions that diverge from the true underlying data distribution. This discrepancy between augmented and authentic data may impact the model's generalizability to unseen instances. Moreover, the augmentation process itself may not fully capture the variability present in real-world data, potentially limiting the model's robustness in handling diverse input scenarios. Furthermore, the choice of augmentation techniques and parameters must be carefully considered to strike a balance between augmentation efficacy and preservation of data integrity. Failure to appropriately calibrate these parameters may inadvertently bias the model towards certain data characteristics, undermining its ability to generalize effectively. Ultimately, while preprocessing serves as a preparatory step in model development, these limitations increment the importance of rigorous validation and sensitivity analyses to ensure the robustness and reliability of classification outcomes.

### 4.3.3   Model Limitations

The model employed in this study for binary classification presents several limitations that merit consideration. Firstly, while a Convolutional Neural Network (CNN) architecture, specifically a 3D convolutional network, is commonly utilized for image-based tasks due to its ability to capture spatial dependencies, it may not be optimally suited for the size and complexity of the dataset. The chosen architecture, comprising multiple convolutional, activation, normalization, and dropout layers, introduces considerable complexity. However, this complexity may impose challenges, particularly when working with relatively limited datasets. Overly complex models run the risk of

overfitting, wherein the model learns to memorize noise or traits in the training data rather than capturing genuine underlying patterns. Moreover, the model's hyperparameters, including learning rate, dropout rate, and regularization strength, were not extensively tuned in this study. Suboptimal hyperparameter settings can hinder the model's performance and convergence, leading to subpar classification outcomes. Additionally, the model's training duration, limited to 30 epochs in Google Colab, may have been insufficient for convergence or optimal performance attainment. Longer training durations or more sophisticated training strategies, such as learning rate scheduling, could potentially enhance model performance. Furthermore, while regularization techniques such as L2 regularization and dropout were incorporated to mitigate overfitting, their efficacy may vary depending on the dataset characteristics and model architecture. Inadequate regularization or improper tuning of regularization parameters may increase overfitting or fail to sufficiently constrain model complexity. Finally, the choice of activation functions, such as Leaky ReLU, and the sigmoid activation in the output layer, may impact the model's representational capacity and convergence properties. Different activation functions exhibit varying degrees of effectiveness in capturing non-linear relationships and mitigating issues like vanishing gradients. Thus, the selection of activation functions warrants careful consideration and empirical validation.

While the chosen model architecture represents a common approach for image classification tasks, its performance and generalizability are contingent on several factors, including dataset characteristics, hyperparameter tuning, and regularization efficacy. Addressing these limitations through rigorous experimentation and optimization can lead to more robust and reliable classification outcomes.

## 4.4   Comparison with Similar Studies

When comparing the proposed model to other studies presented in the Table 4.1, it's essential to focus on the best results achieved by each model, particularly in terms of accuracy, sensitivity, specificity, precision, and AUC. Additionally, attention should be given to the similarity of preprocessing techniques employed in other studies.

Among the listed models, the DenseNet and adapted ResNet model from 2020 achieved an accuracy of 0.88 and an AUC of 0.92, which are comparable to the results obtained by the proposed model. However, the proposed model outperformed the DenseNet and

adapted ResNet model in terms of sensitivity (0.87 vs. 0.86) and precision (0.90 vs. not provided). Another notable model is the ResNet (Post-Fusion-A) from 2024, which attained an accuracy of 0.91, similar to the proposed model. However, the proposed model exhibited higher precision (0.90 vs. 0.91).

Regarding preprocessing techniques, the DenseNet and adapted ResNet model, as well as the ResNet (Post-Fusion-A) model, employed similar preprocessing steps, including skull stripping or brain extraction. However, it's worth noting that the proposed model also utilized data augmentation techniques, such as flipping or scaling, which may have contributed to its performance improvement.

Moreover, when comparing the proposed model to other models, particularly those utilizing the OASIS dataset, it's crucial to consider performance metrics and preprocessing techniques. One of the notable models in the table is the 3D CNN (inspired by VGG-16) from 2020, which reported an accuracy of 0.69. In contrast, the proposed model achieved a significantly higher accuracy of 0.91, indicating superior classification performance. While both models utilized the OASIS dataset, the proposed model's superior accuracy suggests that its architecture or preprocessing techniques may have been more effective.

Another relevant comparison can be made with the 3D CNN model from 2021, also utilizing the OASIS dataset. This model reported an AUC of 0.78, lower than the AUC of 0.96 achieved by the proposed model. The considerable difference in AUC values suggests that the proposed model has better discriminatory power in distinguishing between healthy controls and individuals with Alzheimer's disease.

Overall, while several models in the table achieved comparable results to the proposed model in terms of accuracy and AUC, the proposed model demonstrated good sensitivity and precision. Additionally, the inclusion of data augmentation techniques may have contributed to the improved performance of the proposed model compared to models with similar preprocessing techniques. Furthermore, the proposed model demonstrates superior performance compared to other models utilizing the OASIS dataset. This suggests that the proposed model's architecture and/or preprocessing techniques may be more effective in capturing relevant features for Alzheimer's disease classification from MRI data.

| Model | Year | Dataset | Pre-processing | | | Results | | | | | Ref |
|---|---|---|---|---|---|---|---|---|---|---|---|
| | | | Skull stripping/ Brain extraction | Data Augmentation | Segmentation | Accuracy | Sensitivity | Specificity | Precision | AUC | |
| ResNet | 2024 | OASIS 3 | x | x | | 0.8 | 0.8 | - | 0.59 | 0.81 | [97] |
| 3D-Autoencoder | 2019 | ADNI | x | | | 0.93. | - | - | - | | [81] |
| 5 CN layers and 44 channels | 2023 | ADNI | x | | x | 0.87 | - | - | - | - | [82] |
| 12 repeated blocks of 3D CNNs | 2019 | ADNI + Milan | | x | x | 0.98 | 0.98 | 0.98 | - | | [85] |
| DenseNet and adapted ResNet | 2020 | ADNI | x | x | x | 0.88 | 0.86 | 0.9 | - | 0.92 | [98] |
| Multi-task deep CNN | 2020 | ADNI | x | | | 0.8 | 0.79 | 0.8 | - | 0.86 | [98] |
| DenseNet | 2020 | ADNI | x | | | 0.86 | 0.79 | 0.92 | - | 0.87 | [98] |
| ResNet | 2017 | ADNI | x | | | 0.8 | - | - | - | 0.87 | [99] |
| 3D CNN (test 1) | 2018 | ADNI | | x | | 0.82 | 0.88 | 0.85 | - | - | [100] |
| 2D CNN (VGG11 as backbone) | 2020 | ADNI | x | | | 0.92 | 0.85 | - | 0.97 | - | [101] |
| LeNet | 2016 | ADNI | x | | x | 0.98 | - | - | - | - | [94] |
| GoogleNet | 2016 | ADNI | x | | x | 0.98 | - | - | - | - | [94] |
| 3D CNN (inspired by VGG-16) | 2020 | OASIS | x | | | 0.69 | - | - | - | - | [75] |
| 3D CNN | 2021 | OASIS | | | | - | - | - | - | 0.78 | [76] |
| 2D CNN | 2023 | MIRIAD | x | x | x | 0.89 | - | - | - | 0.92 | [95] |
| ResNet (Post-Fusion-A) | 2024 | ADNI | x | | | 0.91 | 0.87 | - | 0.91 | 0.9 | [96] |
| SVM Classifier (Post-Fusion) | 2024 | ADNI | x | | | 0.78 | 0.81 | - | 0.8 | 0.83 | [96] |
| 3D-CNN + Softmax | 2022 | Kaggle, ADNI, | x | x | x | 0.98 | - | - | - | - | [97] |
| 3D-CNN + SVM | 2022 | Kaggle, ADNI, | x | x | x | 0.91 | - | - | - | - | [97] |
| 3D-CNN + RF | 2022 | Kaggle, ADNI, | x | x | x | 0.85 | - | - | - | - | [97] |
| 3D CNN (SVM) | 2022 | ADNI | | | | 0.81 | 0.-82 | 0.78 | - | - | [98] |
| 3D CNN (SAE) | 2022 | ADNI | | | | 0.82 | 0.86 | 0.77 | - | - | [98] |
| eResNet50, eNASNet, eMobileNet | 2019 | ADNI | | | x | 0.98 | 0.97 | 1 | - | - | [99] |
| Hypergraph (SVM classifier) | 2020 | ADNI | | | | 0.88 | 0.9 | 0.85 | - | 0.91 | [100] |
| **Proposed Model** | **2024** | **OASIS 3** | **x** | **x** | **x** | **0.91** | **0.87** | **0.93** | **0.9** | **0.96** | |

Table 4.1 Comparison of Binary Classification Models for Alzheimer's Disease Detection Using MRI Data

# Chapter 5

# Conclusions and Outlook

In the realm of neurodegenerative diseases, Alzheimer's disease is a significant challenge, affecting millions globally and causing a profound socio-economic impact. Therefore, there is a pressing need to improve diagnostic methods for Alzheimer's disease. Early and accurate diagnosis is paramount for timely intervention, offering a window of opportunity to implement strategies that may slow down the progression of the disease. In this context, the study explores the utility of T1-weighted MRI in Alzheimer's diagnosis, focusing on binary classification as a practical approach given the computational constraints.

Medical imaging, particularly MRI, has become a valuable tool in neuroimaging, providing detailed information about the brain and its structure. The non-invasiveness and high resolution of MRI make it indispensable in Alzheimer's research. Its ability to capture structural changes and abnormalities in brain tissues allows for a better understanding of the disease progression, facilitating early detection and intervention. Consequently, advancements in MRI techniques contribute significantly to improving Alzheimer's diagnosis.

Pre-processing and data augmentation play an important role on increasing the efficacy of machine learning models for medical image analysis. The complexity and variability of medical images needs careful pre-processing to enhance the model's ability to detect

subtle patterns. Data augmentation further helps in diversifying the training dataset, promoting robustness and generalization. In Alzheimer's diagnosis, these pre-processing steps are significant for extracting meaningful features and improving the model's ability to differentiate between healthy and affected brain structures.

Segmentation, a principal characteristic of this model's pre-processing pipeline, involves defining distinct brain regions. This process contributes to a better analysis, allowing the model to focus on specific areas implicated in Alzheimer's pathology. By isolating relevant structures, the model potentially enhances diagnostic accuracy. The segmentation method used in this study was both easy to use and effective within time and computational constraints.

The simplicity of the proposed model, rooted in binary classification shows the practical approach of the study. Despite its simplicity and training in limited number of epochs, the model demonstrates excellent results when compared with similar models.

However, despite the study's promise, it faces limitations that deserve attention. Firstly, the dataset used in the project from the OASIS 3 database presents challenges due to class imbalance and lack of diversity, potentially limiting the model's generalizability and feature extraction capabilities. Additionally, preprocessing steps such as brain segmentation using FSL and data augmentation techniques introduce complexities that require careful consideration to maintain data integrity and ensure model robustness.

The model's architecture, while commonly used, might not be optimally suited for the dataset's size and complexity. The complexity introduced by multiple layers may pose challenges, especially with relatively limited datasets, potentially leading to overfitting. Additionally, the proposed model's hyperparameters were not extensively fine-tuned, which could affect its performance and convergence. The limited training duration could also have prevented optimal performance.

Furthermore, although the current study has identified several limitations, it still offers promising results. Therefore, the potential of the proposed model can be further explored through parameter tuning and validation techniques. Implementing grid search and k-fold cross-validation would offer a more detailed understanding of the model's performance across diverse datasets, which in turn would offer possible avenues to

address the previously mentioned limitations. Additionally, considering the complexity of the OASIS 3 dataset, conducting training simultaneously on different MRI sequences could provide a better perspective, contributing to a robust and versatile diagnostic tool.

The proposed model shows significant potential in diagnosing Alzheimer's through T1-weighted MRI scans. The urgency to improve diagnostic abilities for Alzheimer's is emphasized by the significant impact of the disease. The study highlights the big role of MRI in providing detailed information of brain structures, with pre-processing steps such as segmentation and data augmentation contributing to the model's efficacy. While the simplicity of the model is acknowledged, its robust performance indicates its potential for further refinement. By integrating advanced techniques and exploring varied data augmentation methods, we can increment the model's diagnostic capacity, advancing toward more precise and dependable Alzheimer's diagnoses.

## 5.1  Future Work

Looking toward the future, the landscape of Alzheimer's diagnosis using neuroimaging offers a lot opportunities for improvement and refinement. Beyond the specific model proposed in this study, a more generalized approach to advancing diagnostic procedures involves the exploration of various strategies.

Expanding data augmentation techniques stands out as a key avenue for improvement. While the study employed a set of augmentation methods, expanding the dataset to include an even bigger array of transformations, such as spatial deformations, color augmentations, and more, can enrich the dataset. By exposing the model to a variety of scenarios, the augmented dataset becomes more representative of the variability encountered in clinical settings, enhancing the model's adaptability.

The evaluation of different pre-processing pipelines remains a vital aspect of enhancing diagnostic models. Beyond segmentation, which was a focal point in the proposed model, investigating alternative pre-processing techniques, including normalization, intensity correction, and feature extraction methods, can contribute to more refined and informative input for the model. Comparative analyses of these pre-processing strategies can show their respective impacts on model performance.

Moreover, expanding beyond binary to multi-class classification presents the realistic progression of Alzheimer's disease. Considering the spectrum of disease severity allows for a finer categorization of patients, potentially enabling more personalized interventions. Additionally, the inclusion of more classes could shed light on the intermediate stages of the disease, aiding in the identification of early biomarkers.

The enhancement of Alzheimer's diagnosis through neuroimaging requires a thorough and forward-thinking approach. Advancements in data augmentation, pre-processing, dataset diversity, classification strategies, analysis levels, longitudinal studies, and predictive modeling collectively contribute to a comprehensive diagnostic framework. Continuous exploration and innovation in these dimensions hold the potential not only to improve models but to transform how Alzheimer's diagnosis is approached, leading to more effective and personalized treatments.

### 5.1.1   Web Application

In addition to the findings and conclusions presented in this study, there are several avenues for future research and development that could further enhance the impact and usability of the proposed model. One such avenue involves the development of a web application (Fig. 5.1) aimed at facilitating interaction between healthcare professionals and patients based on the model's diagnosis.
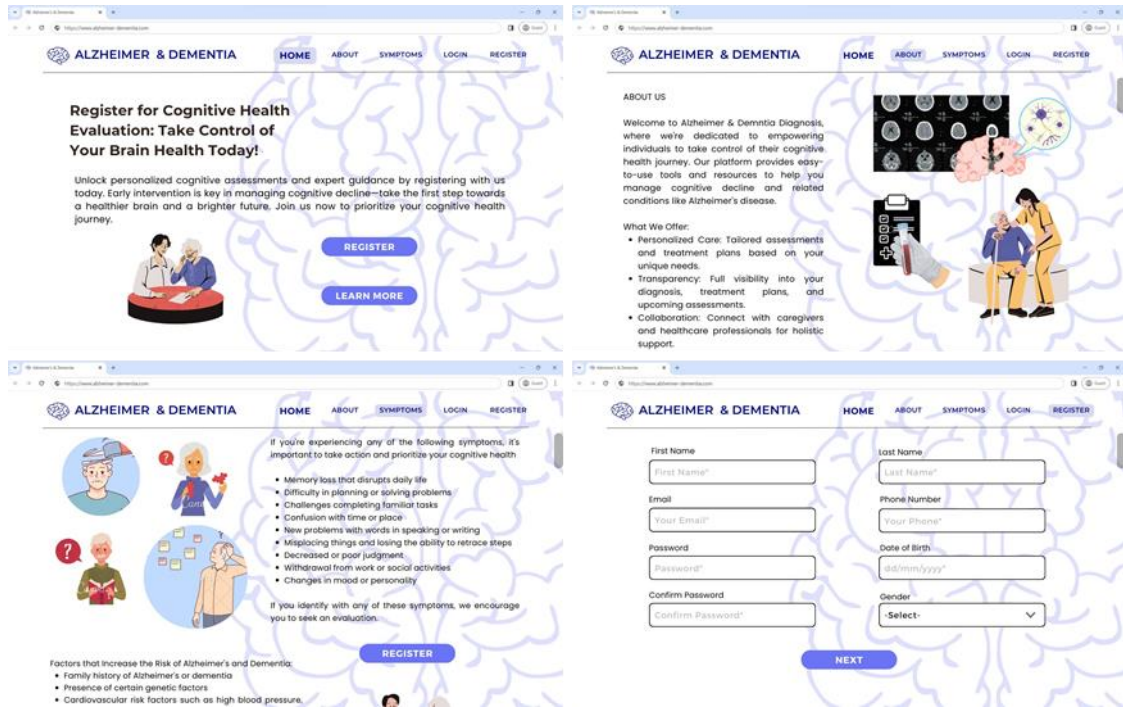
Figure 5.1 Proposed Web Application, view of Home, About, Symptoms and Register pages.

At the core of this proposal lies the development of a user-friendly web platform where physicians can easily upload MRI NIfTI files for analysis (Fig 5.2). Using the advancements in deep learning and medical imaging, the application will employ a trained model specifically designed for Alzheimer's disease diagnosis. Through the integration of this model, physicians will gain access to a sophisticated diagnostic tool capable of providing accurate and timely assessments based on MRI scans.



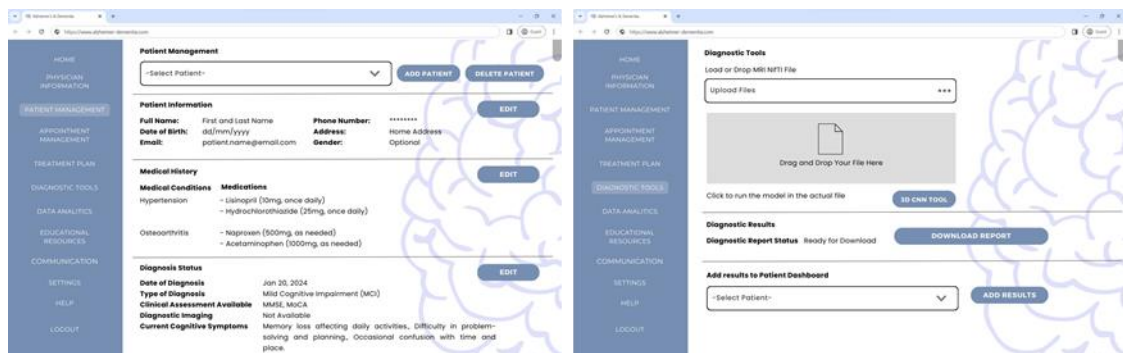Figure 5.2 Proposed Web Application, view of Physician Dashboard

Upon accessing the web application, physicians will be greeted with a straightforward interface designed for an easy navigation. The platform will offer intuitive functionalities, allowing physicians to register patients and upload their MRI scans with ease. Once the MRI scans are uploaded, the trained model will rapidly analyze the

images, extracting pertinent features and patterns indicative of AD. Employing state-of-the-art CNNs, the model will deliver comprehensive diagnostic reports, detailing key metrics such as classification accuracy, sensitivity, specificity, precision, and AUC. These reports will serve as invaluable resources for physicians, aiding in informed decision-making and personalized patient care.

Furthermore, the web application will extend its functionalities beyond diagnosis, catering to the needs of both physicians and patients. For patients, the platform will offer a personalized dashboard where they can access their diagnosis status, review past appointments, schedule future consultations, and access educational resources related to AD management (Fig 5.3).
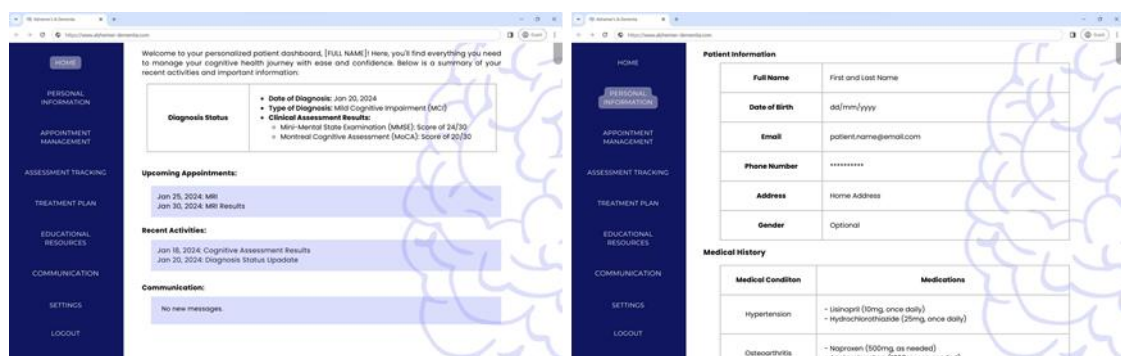


Figure 5.3 Proposed Web Application, view of Patient Dashboard

Additionally, the web application will feature administrative tools, allowing healthcare professionals to manage patient records, track appointment schedules, and collaborate with colleagues.

The proposed web application represents a tool in the realm of AD diagnosis and management. By utilizing deep learning and medical imaging, the application promises to transform the diagnostic process, enabling physicians to make timely and accurate assessments while empowering patients with personalized information of their health. By fitting into clinical routines and focusing on patients' needs, the web application is positioned to greatly influence how Alzheimer's disease is diagnosed and handled in clinical settings.

# References

[1]     A. P. Skaria, "The Economic and Societal Burden of AlzheimerDisease: Managed Care Considerations," *Am. J. Manag. Care*, vol. 28, pp. S188–S196, Sep. 2022, doi: 10.37765/AJMC.2022.89236.

[2]     N. V. Dokholyan, R. C. Mohs, and R. J. Bateman, "Challenges and progress in research, diagnostics, and therapeutics in Alzheimer's disease and related dementias," *Alzheimer's Dement. Transl. Res. Clin. Interv.*, vol. 8, no. 1, 2022, doi: 10.1002/TRC2.12330.

[3]     B. K. Beata, J. Wojciech, K. Johannes, L. Piotr, and M. Barbara, "Alzheimer's Disease— Biochemical and Psychological Background for Diagnosis and Treatment," *Int. J. Mol. Sci.*, vol. 24, no. 2, Jan. 2023, doi: 10.3390/IJMS24021059.

[4]     A. P. Porsteinsson, R. S. Isaacson, S. Knox, M. N. Sabbagh, and I. Rubino, "Diagnosis of Early Alzheimer's Disease: Clinical Practice in 2021," *J. Prev. Alzheimer's Dis. 2021 83*, vol. 8, no. 3, pp. 371–386, Jun. 2021, doi: 10.14283/JPAD.2021.23.

[5]     B. Dubois *et al.*, "Clinical diagnosis of Alzheimer's disease: recommendations of the International Working Group," *Lancet Neurol.*, vol. 20, no. 6, pp. 484–496, Jun. 2021, doi: 10.1016/S1474-4422(21)00066-1.

[6]     P. M. Rossini *et al.*, "Early diagnosis of Alzheimer's disease: the role of biomarkers including advanced EEG signal analysis. Report from the IFCN-sponsored panel of experts," *Clin. Neurophysiol.*, vol. 131, no. 6, pp. 1287–1310, Jun. 2020, doi: 10.1016/J.CLINPH.2020.03.003.

[7]     S. Gao and D. Lima, "A review of the application of deep learning in the detection of Alzheimer's disease," *Int. J. Cogn. Comput. Eng.*, vol. 3, pp. 1–8, Jun. 2022, doi: 10.1016/J.IJCCE.2021.12.002.

[8]     S. P. Singh, L. Wang, S. Gupta, H. Goli, P. Padmanabhan, and B. Gulyás, "3D Deep Learning on Medical Images: A Review," *Sensors 2020, Vol. 20, Page 5097*, vol. 20, no. 18, p. 5097, Sep. 2020, doi: 10.3390/S20185097.

[9]     "Alzheimer's Disease Fact Sheet | National Institute on Aging." Accessed: Jan. 25, 2024. [Online]. Available: https://www.nia.nih.gov/health/alzheimers-and-dementia/alzheimers-disease-fact-sheet

[10]    C. Greenblat, "Dementia," World Health Organization. Accessed: Jan. 19, 2024. [Online]. Available: https://www.who.int/news-room/fact-sheets/detail/dementia

[11]    X. Li, X. Feng, X. Sun, N. Hou, F. Han, and Y. Liu, "Global, regional, and national burden of Alzheimer's disease and other dementias, 1990–2019," *Front. Aging Neurosci.*, vol. 14, p. 937486, Oct. 2022, doi: 10.3389/FNAGI.2022.937486.

[12]    "Prevalence of Alzheimer's disease and other dementias." Our World In Data. [Online]. Available: https://ourworldindata.org/grapher/prevalence-of-dementias

[13]    D. E. Ball *et al.*, "A framework for addressing Alzheimer's disease: Without a frame, the work has no aim," *Alzheimer's Dement.*, vol. 19, no. 4, pp. 1568–1578, Apr. 2023, doi: 10.1002/ALZ.12869.

[14]    "2023 Alzheimer's disease facts and figures," *Alzheimer's Dement.*, vol. 19, no. 4, pp. 1598–1695, Apr. 2023, doi: 10.1002/ALZ.13016.

[15]    A. Nandi *et al.*, "Global and regional projections of the economic burden of Alzheimer's disease and related dementias from 2019 to 2050: A value of statistical life approach," *eClinicalMedicine*, vol. 51, p. 101580, Sep. 2022, doi: 10.1016/J.ECLINM.2022.101580.

[16]  Y. Ratan *et al.*, "An Insight into Cellular and Molecular Mechanisms Underlying the Pathogenesis of Neurodegeneration in Alzheimer's Disease," *Biomed. 2023, Vol. 11, Page 1398*, vol. 11, no. 5, p. 1398, May 2023, doi: 10.3390/BIOMEDICINES11051398.

[17]  Q. Wang and C. Xie, "Microglia activation linking amyloid-β drive tau spatial propagation in Alzheimer's disease," *Front. Neurosci.*, vol. 16, Aug. 2022, doi: 10.3389/FNINS.2022.951128.

[18]  J. C. Lee, S. J. Kim, S. Hong, and Y. S. Kim, "Diagnosis of Alzheimer's disease utilizing amyloid and tau as fluid biomarkers," *Exp. Mol. Med. 2019 515*, vol. 51, no. 5, pp. 1–10, May 2019, doi: 10.1038/s12276-019-0250-2.

[19]  J. L. Liss *et al.*, "Practical recommendations for timely, accurate diagnosis of symptomatic Alzheimer's disease (MCI and dementia) in primary care: a review and synthesis," *J. Intern. Med.*, vol. 290, no. 2, pp. 310–334, Aug. 2021, doi: 10.1111/JOIM.13244.

[20]  J. van der Schaar *et al.*, "Considerations regarding a diagnosis of Alzheimer's disease before dementia: a systematic review," *Alzheimers. Res. Ther.*, vol. 14, no. 1, Dec. 2022, doi: 10.1186/S13195-022-00971-3.

[21]  M. Pais *et al.*, "Early diagnosis and treatment of Alzheimer's disease: new definitions and challenges," *Brazilian J. Psychiatry*, vol. 42, no. 4, p. 431, Jul. 2020, doi: 10.1590/1516-4446-2019-0735.

[22]  M. Siddiqui *et al.*, "Screening for Cognitive Impairment in Primary Care: Rationale and Tools," *Mo. Med.*, vol. 120, no. 6, p. 431, 2023, Accessed: Jan. 25, 2024. [Online]. Available: /pmc/articles/PMC10743330/

[23]  J. E. Galvin and C. H. Sadowsky, "Practical Guidelines for the Recognition and Diagnosis of Dementia," *J. Am. Board Fam.    Med.*, vol. 25, no. 3, pp. 367–382, May 2012, doi: 10.3122/JABFM.2012.03.100181.

[24]  Z. Arvanitakis, R. C. Shah, and D. A. Bennett, "Diagnosis and Management of Dementia: A Review," *JAMA*, vol. 322, no. 16, p. 1589, Oct. 2019, doi: 10.1001/JAMA.2019.4782.

[25]  K. R. Scott and A. M. Barrett, "Dementia syndromes: evaluation and treatment," *Expert Rev. Neurother.*, vol. 7, no. 4, p. 407, Apr. 2007, doi: 10.1586/14737175.7.4.407.

[26]  S. Gauthier, P. Rosa-Neto, J. A. Morais, and C. Webster, "World Alzheimer Report 2021: Journey through the diagnosis of dementia," *Alzheimer's Dis. Int.*, 2021.

[27]  M. Te Pas, M. O. Rikkert, A. Bouwman, R. Kessels, and M. Buise, "Screening for Mild Cognitive Impairment in the Preoperative Setting: A Narrative Review," *Healthc. 2022, Vol. 10, Page 1112*, vol. 10, no. 6, p. 1112, Jun. 2022, doi: 10.3390/HEALTHCARE10061112.

[28]  "A guide to detecting cognitive impairment during the Medicare Annual Wellness Visit COGNITIVE ASSESSMENT TOOLKIT," *Alzheimer's Assoc.*.

[29]  R. J. Jutten *et al.*, "Detecting functional decline from normal aging to dementia: Development and validation of a short version of the Amsterdam IADL Questionnaire," *Alzheimer's Dement.    Diagnosis, Assess. Dis. Monit.*, vol. 8, p. 26, 2017, doi: 10.1016/J.DADM.2017.03.002.

[30]  A. L. Teixeira, N. P. Rocha, and J. Gatchel, "Behavioral or neuropsychiatric symptoms of Alzheimer's disease: from psychopathology to pharmacological management," *Arq. Neuropsiquiatr.*, vol. 81, no. 12, p. 1152, 2023, doi: 10.1055/S-0043-1777774.

[31]  J. M. Ringman *et al.*, "Early behavioural changes in familial Alzheimer's disease in the Dominantly Inherited Alzheimer Network," *Brain*, vol. 138, no. 4, pp. 1036–1045, Apr. 2015, doi: 10.1093/BRAIN/AWV004.

[32]  H. M. Zeng, H. B. Han, Q. F. Zhang, and H. Bai, "Application of modern neuroimaging technology in the diagnosis and study of Alzheimer's disease," *Neural Regen. Res.*, vol. 16, no. 1, p. 73, Jan. 2021, doi: 10.4103/1673-5374.286957.

[33]  P. A. Rowley, A. A. Samsonov, T. J. Betthauser, A. Pirasteh, S. C. Johnson, and L. B. Eisenmenger, "Amyloid and Tau PET Imaging of Alzheimer Disease and Other Neurodegenerative Conditions," *Semin. Ultrasound, CT MRI*, vol. 41, no. 6, pp. 572–583,

Dec. 2020, doi: 10.1053/J.SULT.2020.08.011.

[34]    A. Dave, N. Hansen, R. Downey, and C. Johnson, "FDG-PET Imaging of Dementia and Neurodegenerative Disease," *Semin. Ultrasound, CT MRI*, vol. 41, no. 6, pp. 562–571, Dec. 2020, doi: 10.1053/J.SULT.2020.08.010.

[35]    C. G. Schwarz, "Uses of Human MR and PET Imaging in Research of Neurodegenerative Brain Diseases," *Neurother. 2021 182*, vol. 18, no. 2, pp. 661–672, Mar. 2021, doi: 10.1007/S13311-021-01030-9.

[36]    S. D. K., S. N. Joshi, V. H. Kumar, V. Venkataramanan, and K. C. S., "A Review on Neural Networks and its Applications," *J. Comput. Technol. Appl.*, vol. 14, no. 2, pp. 59–70, 2023, doi: 10.37591/jocta.v14i2.1062.

[37]    A. Thakur, "Fundamentals of Neural Networks," *Int. J. Res. Appl. Sci. Eng. Technol.*, vol. 9, no. VIII, pp. 407–426, Aug. 2021, doi: 10.22214/ijraset.2021.37362.

[38]    A. Anaya-Isaza, L. Mera-Jiménez, and M. Zequera-Diaz, "An overview of deep learning in medical imaging," *Informatics Med. Unlocked*, vol. 26, p. 100723, Jan. 2021, doi: 10.1016/J.IMU.2021.100723.

[39]    M. M. Taye, "Theoretical Understanding of Convolutional Neural Network: Concepts, Architectures, Applications, Future Directions," *Comput. 2023, Vol. 11, Page 52*, vol. 11, no. 3, p. 52, Mar. 2023, doi: 10.3390/COMPUTATION11030052.

[40]    S. Kiranyaz, O. Avci, O. Abdeljaber, T. Ince, M. Gabbouj, and D. J. Inman, "1D convolutional neural networks and applications: A survey," *Mech. Syst. Signal Process.*, vol. 151, p. 107398, Apr. 2021, doi: 10.1016/J.YMSSP.2020.107398.

[41]    S. Badillo *et al.*, "An Introduction to Machine Learning," *Clin. Pharmacol. Ther.*, vol. 107, no. 4, pp. 871–885, Apr. 2020, doi: 10.1002/CPT.1796.

[42]    L. Alzubaidi *et al.*, "Review of deep learning: concepts, CNN architectures, challenges, applications, future directions," *J. Big Data 2021 81*, vol. 8, no. 1, pp. 1–74, Mar. 2021, doi: 10.1186/S40537-021-00444-8.

[43]    T. K. Gupta and K. Raza, "Optimization of ANN Architecture: A Review on Nature-Inspired Techniques," *Mach. Learn. Bio-Signal Anal. Diagnostic Imaging*, pp. 159–182, Jan. 2019, doi: 10.1016/B978-0-12-816086-2.00007-2.

[44]    M. Abbas, I. Cho, and J. Kim, "Recursive multilayer perceptron-based data-driven identification for a parameterized polarization model of rechargeable Li-ion battery," *Appl. Soft Comput.*, vol. 101, p. 107073, Mar. 2021, doi: 10.1016/J.ASOC.2020.107073.

[45]    J. Chaki, N. Dey, L. Moraru, and F. Shi, "Fragmented plant leaf recognition: Bag-of-features, fuzzy-color and edge-texture histogram descriptors with multi-layer perceptron," *Optik (Stuttg).*, vol. 181, pp. 639–650, Mar. 2019, doi: 10.1016/J.IJLEO.2018.12.107.

[46]    H. Amakdouf, M. El Mallahi, A. Zouhri, A. Tahiri, and H. Qjidaa, "Classification and Recognition of 3D Image of Charlier moments using a Multilayer Perceptron Architecture," *Procedia Comput. Sci.*, vol. 127, pp. 226–235, Jan. 2018, doi: 10.1016/J.PROCS.2018.01.118.

[47]    Z. Qiu, E. Lazar, and K. Nakata, "VaR and ES forecasting via recurrent neural network-based stateful models," *Int. Rev. Financ. Anal.*, vol. 92, p. 103102, Mar. 2024, doi: 10.1016/J.IRFA.2024.103102.

[48]    T. Fang, C. Zheng, and D. Wang, "Forecasting the crude oil prices with an EMD-ISBM-FNN model," *Energy*, vol. 263, p. 125407, Jan. 2023, doi: 10.1016/J.ENERGY.2022.125407.

[49]    F. Zhou, H. min Zhou, Z. Yang, and L. Yang, "EMD2FNN: A strategy combining empirical mode decomposition and factorization machine based neural network for stock market trend prediction," *Expert Syst. Appl.*, vol. 115, pp. 136–151, Jan. 2019, doi: 10.1016/J.ESWA.2018.07.065.

[50]    J. T. Chien and A. Misbullah, "Deep long short-term memory networks for speech recognition," *Proc. 2016 10th Int. Symp. Chinese Spok. Lang. Process. ISCSLP 2016*, May 2017, doi: 10.1109/ISCSLP.2016.7918375.

[51]    M. Malik, M. K. Malik, K. Mehmood, and I. Makhdoom, "Automatic speech recognition: a survey," *Multimed. Tools Appl.*, vol. 80, no. 6, pp. 9411–9457, Mar. 2021, doi: 10.1007/S11042-020-10073-7/METRICS.

[52]    I. Rizwan I Haque and J. Neubert, "Deep learning approaches to biomedical image segmentation," *Informatics Med. Unlocked*, vol. 18, p. 100297, Jan. 2020, doi: 10.1016/J.IMU.2020.100297.

[53]    T. K. Dutta, D. R. Nayak, and Y. D. Zhang, "ARM-Net: Attention-guided residual multiscale CNN for multiclass brain tumor classification using MR images," *Biomed. Signal Process. Control*, vol. 87, p. 105421, Jan. 2024, doi: 10.1016/J.BSPC.2023.105421.

[54]    S. Saifullah and R. Dreżewski, "Modified Histogram Equalization for Improved CNN Medical Image Segmentation," *Procedia Comput. Sci.*, vol. 225, pp. 3021–3030, Jan. 2023, doi: 10.1016/J.PROCS.2023.10.295.

[55]    E. Tsalera, A. Papadakis, I. Voyiatzis, and M. Samarakou, "CNN-based, contextualized, real-time fire detection in computational resource-constrained environments," *Energy Reports*, vol. 9, pp. 247–257, Sep. 2023, doi: 10.1016/J.EGYR.2023.05.260.

[56]    A. I. Jabbooree, L. M. Khanli, P. Salehpour, and S. Pourbahrami, "A novel facial expression recognition algorithm using geometry β –skeleton in fusion based on deep CNN," *Image Vis. Comput.*, vol. 134, p. 104677, Jun. 2023, doi: 10.1016/J.IMAVIS.2023.104677.

[57]    R. DiPietro and G. D. Hager, "Deep learning: RNNs and LSTM," *Handb. Med. Image Comput. Comput. Assist. Interv.*, pp. 503–519, Jan. 2020, doi: 10.1016/B978-0-12-816176-0.00026-0.

[58]    S. M. Lakew, M. C. Fondazione, B. Kessler, M. Federico, M. Srl, and T. Fondazione, "A Comparison of Transformer and Recurrent Neural Networks on Multilingual Neural Machine Translation," *COLING 2018 - 27th Int. Conf. Comput. Linguist. Proc.*, pp. 641–652, Jun. 2018, Accessed: Jan. 25, 2024. [Online]. Available: https://arxiv.org/abs/1806.06957v2

[59]    I. Sheikh, E. Vincent, and I. Illina, "Training RNN language models on uncertain ASR hypotheses in limited data scenarios," *Comput. Speech Lang.*, vol. 83, p. 101555, Jan. 2024, doi: 10.1016/J.CSL.2023.101555.

[60]    A. S. Saud and S. Shakya, "Analysis of look back period for stock price prediction with RNN variants: A case study on banking sector of NEPSE," *Procedia Comput. Sci.*, vol. 167, pp. 788–798, Jan. 2020, doi: 10.1016/J.PROCS.2020.03.419.

[61]    V. Lempitsky, "Autoencoder," *Comput. Vis.*, pp. 1–6, 2020, doi: 10.1007/978-3-030-03243-2_862-1.

[62]    K. Yang, S. Kim, and J. B. Harley, "Unsupervised long-term damage detection in an uncontrolled environment through optimal autoencoder," *Mech. Syst. Signal Process.*, vol. 199, p. 110473, Sep. 2023, doi: 10.1016/J.YMSSP.2023.110473.

[63]    S. Chaudhuri, S. Ghosh, D. Dey, S. Munshi, B. Chatterjee, and S. Dalai, "Denoising of partial discharge signal using a hybrid framework of total variation denoising-autoencoder," *Measurement*, vol. 223, p. 113674, Dec. 2023, doi: 10.1016/J.MEASUREMENT.2023.113674.

[64]    F. Samann and T. Schanze, "RunDAE model: Running denoising autoencoder models for denoising ECG signals," *Comput. Biol. Med.*, vol. 166, p. 107553, Nov. 2023, doi: 10.1016/J.COMPBIOMED.2023.107553.

[65]    K. Shinde, V. Itier, J. Mennesson, D. Vasiukov, and M. Shakoor, "Dimensionality reduction through convolutional autoencoders for fracture patterns prediction," *Appl. Math. Model.*, vol. 114, pp. 94–113, Feb. 2023, doi: 10.1016/J.APM.2022.09.034.

[66]    X. Ran, W. Chen, B. Yvert, and S. Zhang, "A hybrid autoencoder framework of dimensionality reduction for brain-computer interface decoding," *Comput. Biol. Med.*, vol. 148, p. 105871, Sep. 2022, doi: 10.1016/J.COMPBIOMED.2022.105871.

[67]    A. Creswell, T. White, V. Dumoulin, K. Arulkumaran, B. Sengupta, and A. A. Bharath,

"Generative Adversarial Networks: An Overview," *IEEE Signal Process. Mag.*, vol. 35, no. 1, pp. 53–65, Jan. 2018, doi: 10.1109/MSP.2017.2765202.

[68]    L. Wang, W. Chen, W. Yang, F. Bi, and F. R. Yu, "A State-of-the-Art Review on Image Synthesis with Generative Adversarial Networks," *IEEE Access*, vol. 8, pp. 63514–63537, 2020, doi: 10.1109/ACCESS.2020.2982224.

[69]    S. Rani, D. Jining, D. Shah, S. Xaba, and P. R. Singh, "The Role of Artificial Intelligence in Art: A Comprehensive Review of a Generative Adversarial Network Portrait Painting," pp. 126–135, 2023, doi: 10.1007/978-3-031-50330-6_13/COVER.

[70]    J. Gutierrez and J. Schrum, "Generative Adversarial Network Rooms in Generative Graph Grammar Dungeons for the Legend of Zelda," *2020 IEEE Congr. Evol. Comput. CEC 2020 - Conf. Proc.*, Jul. 2020, doi: 10.1109/CEC48606.2020.9185631.

[71]    N. J. Avanaki, S. Zadtootaghaj, N. Barman, S. Schmidt, M. G. Martini, and S. Moller, "Quality Enhancement of Gaming Content using Generative Adversarial Networks," *2020 12th Int. Conf. Qual. Multimed. Exp. QoMEX 2020*, May 2020, doi: 10.1109/QOMEX48832.2020.9123074.

[72]    S. Mulé *et al.*, "Generative adversarial networks (GAN)-based data augmentation of rare liver cancers: The SFR 2021 Artificial Intelligence Data Challenge," *Diagn. Interv. Imaging*, vol. 104, no. 1, pp. 43–48, Jan. 2023, doi: 10.1016/J.DIII.2022.09.005.

[73]    M. Zhang, Z. Wang, X. Wang, M. Gong, Y. Wu, and H. Li, "Features kept generative adversarial network data augmentation strategy for hyperspectral image classification," *Pattern Recognit.*, vol. 142, p. 109701, Oct. 2023, doi: 10.1016/J.PATCOG.2023.109701.

[74]    S. Vijh, P. Gaurav, and H. M. Pandey, "Hybrid bio-inspired algorithm and convolutional neural network for automatic lung tumor detection," *Neural Comput. Appl.*, vol. 35, no. 33, pp. 23711–23724, Nov. 2023, doi: 10.1007/S00521-020-05362-Z/FIGURES/7.

[75]    M. Woźniak, J. Siłka, and M. Wieczorek, "Deep neural network correlation learning mechanism for CT brain tumor detection," *Neural Comput. Appl.*, vol. 35, no. 20, pp. 14611–14626, Jul. 2023, doi: 10.1007/S00521-021-05841-X.

[76]    Y. Fu, Y. Lei, T. Wang, W. J. Curran, T. Liu, and X. Yang, "A review of deep learning based methods for medical image multi-organ segmentation," *Phys. Medica*, vol. 85, pp. 107–122, May 2021, doi: 10.1016/J.EJMP.2021.05.003.

[77]    A. Ushinsky *et al.*, "A 3d-2d hybrid u-net convolutional neural network approach to prostate organ segmentation of multiparametric MRI," *Am. J. Roentgenol.*, vol. 216, no. 1, pp. 111–116, Jan. 2021, doi: 10.2214/AJR.19.22168/ASSET/IMAGES/LARGE/01_19_22168_02F_CMYK.JPEG.

[78]    M. Nguyen, T. He, L. An, D. C. Alexander, J. Feng, and B. T. T. Yeo, "Predicting Alzheimer's disease progression using deep recurrent neural networks," *Neuroimage*, vol. 222, p. 117203, Nov. 2020, doi: 10.1016/J.NEUROIMAGE.2020.117203.

[79]    T. Wang, R. G. Qiu, and M. Yu, "Predictive Modeling of the Progression of Alzheimer's Disease with Recurrent Neural Networks," *Sci. Reports 2018 81*, vol. 8, no. 1, pp. 1–12, Jun. 2018, doi: 10.1038/s41598-018-27337-w.

[80]    M. Raju, V. P. Gopi, and V. S. Anitha, "Multi-class Classification of Alzheimer's Disease using 3DCNN Features and Multilayer Perceptron," *2021 Int. Conf. Wirel. Commun. Signal Process. Networking, WiSPNET 2021*, pp. 368–373, Mar. 2021, doi: 10.1109/WISPNET51692.2021.9419393.

[81]    K. R. Kruthika, Rajeswari, and H. D. Maheshappa, "CBIR system using Capsule Networks and 3D CNN for Alzheimer's disease diagnosis," *Informatics Med. Unlocked*, vol. 14, pp. 59–68, Jan. 2019, doi: 10.1016/J.IMU.2018.12.001.

[82]    D. Wang *et al.*, "Deep neural network heatmaps capture Alzheimer's disease patterns reported in a large meta-analysis of neuroimaging studies," *Neuroimage*, vol. 269, p. 119929, Apr. 2023, doi: 10.1016/J.NEUROIMAGE.2023.119929.

[83]    E. Yagis, L. Citi, S. Diciotti, C. Marzi, S. Workalemahu Atnafu, and A. G. S. De Herrera, "3D Convolutional neural networks for diagnosis of alzheimer's disease via structural MRI," *Proc. - IEEE Symp. Comput. Med. Syst.*, vol. 2020-July, pp. 65–70, Jul. 2020, doi:

10.1109/CBMS49503.2020.00020.

[84]   N. J. Dhinagar *et al.*, "3D convolutional neural networks for classification of Alzheimer's and Parkinson's disease with T1-weighted brain MRI," *https://doi.org/10.1117/12.2606297*, vol. 12088, pp. 277–286, Dec. 2021, doi: 10.1117/12.2606297.

[85]   S. Basaia *et al.*, "Automated classification of Alzheimer's disease and mild cognitive impairment using a single MRI and deep neural networks," *NeuroImage Clin.*, vol. 21, p. 101645, Jan. 2019, doi: 10.1016/J.NICL.2018.101645.

[86]   "ADNI | ACCESS DATA." Accessed: Feb. 21, 2024. [Online]. Available: https://adni.loni.usc.edu/data-samples/access-data/

[87]   "AIBL Study ADNI Data." Accessed: Feb. 21, 2024. [Online]. Available: https://aibl.csiro.au/adni/index.html

[88]   "EPAD | European Prevention of Alzheimer's Dementia Consortium." Accessed: Feb. 21, 2024. [Online]. Available: https://ep-ad.org/

[89]   "The Global Alzheimer's Association Interactive Network." Accessed: Feb. 21, 2024. [Online]. Available: https://www.gaain.org/

[90]   "OASIS Brains - Open Access Series of Imaging Studies." Accessed: Jan. 24, 2024. [Online]. Available: https://www.oasis-brains.org/

[91]   Y. Huang, Y. Shan, W. Qin, and G. Zhao, "Apolipoprotein E ε4 accelerates the longitudinal cerebral atrophy in open access series of imaging studies-3 elders without dementia at enrollment," *Front. Aging Neurosci.*, vol. 15, p. 1158579, May 2023, doi: 10.3389/FNAGI.2023.1158579/BIBTEX.

[92]   S. Matsushita *et al.*, "The Association of Metabolic Brain MRI, Amyloid PET, and Clinical Factors: A Study of Alzheimer's Disease and Normal Controls From the Open Access Series of Imaging Studies Dataset," *J. Magn. Reson. Imaging*, 2023, doi: 10.1002/JMRI.28892.

[93]   M. Jenkinson, C. F. Beckmann, T. E. J. Behrens, M. W. Woolrich, and S. M. Smith, "FSL," *Neuroimage*, vol. 62, no. 2, pp. 782–790, Aug. 2012, doi: 10.1016/J.NEUROIMAGE.2011.09.015.

[94]   V. Popescu *et al.*, "Optimizing parameter choice for FSL-Brain Extraction Tool (BET) on 3D T1 images in multiple sclerosis," *Neuroimage*, vol. 61, no. 4, pp. 1484–1494, Jul. 2012, doi: 10.1016/J.NEUROIMAGE.2012.03.074.

[95]   M. Goto *et al.*, "Estimation of intracranial volume: A comparative study between synthetic MRI and FSL-brain extraction tool (BET)2," *J. Clin. Neurosci.*, vol. 79, pp. 178–182, Sep. 2020, doi: 10.1016/J.JOCN.2020.07.024.

[96]   A. E. Maxwell, T. A. Warner, and L. A. Guillén, "Accuracy Assessment in Convolutional Neural Network-Based Deep Learning Remote Sensing Studies—Part 1: Literature Review," *Remote Sens. 2021, Vol. 13, Page 2450*, vol. 13, no. 13, p. 2450, Jun. 2021, doi: 10.3390/RS13132450.

[97]   M. Gravina, A. García-Pedrero, C. Gonzalo-Martín, C. Sansone, and P. Soda, "Multi input - Multi output 3D CNN for dementia severity assessment with incomplete multimodal data," *Artif. Intell. Med.*, p. 102774, Jan. 2024, doi: 10.1016/J.ARTMED.2024.102774.

[98]   M. Liu *et al.*, "A multi-model deep convolutional neural network for automatic hippocampus segmentation and classification in Alzheimer's disease," *Neuroimage*, vol. 208, p. 116459, Mar. 2020, doi: 10.1016/J.NEUROIMAGE.2019.116459.

[99]   S. Korolev, A. Safiullin, M. Belyaev, and Y. Dodonova, "Residual and plain convolutional neural networks for 3D brain MRI classification," *Proc. - Int. Symp. Biomed. Imaging*, pp. 835–838, Jun. 2017, doi: 10.1109/ISBI.2017.7950647.

[100]  A. Khvostikov, K. Aderghal, J. Benois-Pineau, A. Krylov, and G. Catheline, "3D CNN-based classification using sMRI and MD-DTI images for Alzheimer disease studies," Jan. 2018, Accessed: Feb. 22, 2024. [Online]. Available: https://arxiv.org/abs/1801.05968v1

[101]  X. Xing *et al.*, "Dynamic Image for 3D MRI Image Alzheimer's Disease Classification," *Lect. Notes Comput. Sci. (including Subser. Lect. Notes Artif. Intell. Lect. Notes*

*Bioinformatics)*, vol. 12535 LNCS, pp. 355–364, 2020, doi: 10.1007/978-3-030-66415-2_23/COVER.